

## Supporting Information

### **Interparticle Anti-Galvanic Reactions of Atomically Precise Silver Nanoclusters with Plasmonic Gold Nanoparticles: Interfacial Control of Atomic Exchange**

Paulami Bose,<sup>a†</sup> Jayoti Roy,<sup>a</sup> Vikash Khokhar,<sup>a</sup> Biswajit Mondal,<sup>a</sup> Ganapati Natarajan,<sup>b</sup> Sujan Manna,<sup>a</sup> Vivek Yadav,<sup>a</sup> Anupriya Nyayban,<sup>a</sup> Sharma S. R. K. C. Yamijala,<sup>\*c</sup> Nonappa,<sup>\*d</sup> and Thalappil Pradeep <sup>\*a,b</sup>

<sup>a</sup>DST Unit of Nanoscience (DST UNS) and Thematic Unit of Excellence (TUE), Department of Chemistry, Indian Institute of Technology Madras, Chennai 600 036, India.

<sup>b</sup>International Centre for Clean Water, 2<sup>nd</sup> Floor, B-Block, IIT Madras Research Park, Kanagam Road, Taramani, Chennai 600113, India.

<sup>c</sup>Department of Chemistry, Indian Institute of Technology Madras, Chennai 600 036, India.

<sup>†d</sup>Faculty of Engineering and Natural Sciences, Tampere University, FI-33720, Tampere, Finland.

<sup>†</sup>Present Address

\*E-mail: pradeep@iitm.ac.in

#### **Table of Contents**

<b>Name</b>	<b>Description</b>	<b>Page No.</b>
SI 1	Experimental section	4-7
SI 2	Concentration calculations	7-11
Figure S1	Characterization of Au@DMBT NP	11
Figure S2	Characterization of [Ag <sub>25</sub> (DMBT) <sub>18</sub> ] <sup>-</sup> NC	12
Figure S3	Morphology of reacted Au@DMBT NPs	12
Figure S4	Particle size distribution of NPs before and after reaction	13
Figure S5	UV-Vis spectra of reaction@NP for Au@DMBT NP and [Ag <sub>25</sub> (DMBT) <sub>18</sub> ] <sup>-</sup> NC system	13
Figure S6	EDS spectrum of reacted NP	14
Figure S7	Full-range ESI mass spectra of the DMBT-capped-NP and NC reaction	14

Figure S8	Isotopic distribution pattern of assigned species for DMBT-DMBT reaction@NC	15
Figure S9	Photoluminescence spectra of reacted $[\text{Ag}_{25}(\text{DMBT})_{18}]^{-}$ NC	15
Figure S10	ESI MS of reaction@NP and @NC mixture	16
Figure S11	Morphological correlation between reactants and the product	16
Figure S12	Characterization of Au@BDT NP	17
Figure S13	Characterization of $[\text{Ag}_{29}(\text{BDT})_{12}(\text{TPP})_4]^{3-}$ NC	17
Figure S14	UV-Vis spectra of reaction@NP for Au@BDT NP and $[\text{Ag}_{29}(\text{BDT})_{12}(\text{TPP})_4]^{3-}$ NC system	18
Figure S15	TEM images of the reaction@NP mixture for BDT-capped NP-NC reaction with time	18
Figure S16	EDS spectra of BDT-capped NP-NC reaction	19
Figure S17	UV-Vis spectra of reaction@NC for Au@BDT NP and $[\text{Ag}_{29}(\text{BDT})_{12}(\text{TPP})_4]^{3-}$ NC system	19
Figure S18	Characterization of $[\text{PPh}_4]_n[\text{Ag}_{44}(\text{FTP})_{30}] \text{NC}$	20
Figure S19	UV-Vis spectra of reaction@NP for Au@DMBT NP and $[\text{Ag}_{44}(\text{FTP})_{30}]^{4-}$ NC system	20
Figure S20	Morphology of Au@DMBT NP before and after reaction with $[\text{Ag}_{44}(\text{FTP})_{30}]^{4-}$ NC system	21
Figure S21	Isotopic distribution pattern of assigned species for DMBT-FTP NC-side reaction	21
Figure S22	UV-Vis spectra of reaction@NC for Au@DMBT NP and $[\text{Ag}_{44}(\text{FTP})_{30}]^{4-}$ NC system	22
Figure S23	Raman studies on reacted Au NP	22
Figure S24	UV-Vis spectra of reaction@NC for Au@BDT NP and $[\text{Ag}_{25}(\text{DMBT})_{18}]^{-}$ NC system	23
Figure S25	Morphology of Au@BDT NP before and after reaction with $[\text{Ag}_{25}(\text{DMBT})_{18}]^{-}$ NC system	23
Figure S26	UV-Vis spectra of reaction@NP for Au@BDT NP and $[\text{Ag}_{25}(\text{DMBT})_{18}]^{-}$ NC system	24
Figure S27	Morphology of Au@DMBT NP before and after reaction with $[\text{Ag}_{29}(\text{BDT})_{12}(\text{TPP})_4]^{3-}$ NC system	24

Figure S28	UV-Vis spectra of reaction@NP for Au@DMBT NP and [Ag <sub>29</sub> (BDT) <sub>12</sub> (TPP) <sub>4</sub> ] <sup>3-</sup> NC system	25
Figure S29	ESI mass spectra for the reaction@NC for Au@DMBT NP and [Ag <sub>29</sub> (BDT) <sub>12</sub> (TPP) <sub>4</sub> ] <sup>3-</sup> NC system	25
Figure S30	UV-Vis spectra for the reaction@NC for Au@DMBT NP and [Ag <sub>29</sub> (BDT) <sub>12</sub> (TPP) <sub>4</sub> ] <sup>3-</sup> NC system	26
Figure S31	Interparticle reaction between Au@BDT NP and [PPh <sub>4</sub> ] <sub>n</sub> [Ag <sub>44</sub> (FTP) <sub>30</sub> ] NC	27
SI 3	Computational details	28
SI 4	Au(111)@SR surface construction	29
Figure S32	Surface construction of Au(111)@SR surfaces	29
Figure S33	Ligand orientations at full coverage on Au(111) surface	30
SI 5	Ag NC–Au(111)@SR docking interactions	30
Figure S34	Optimized Au(111)@SR surface with partial ligand coverage	31
SI 6	Ligand coverage calculation	31
Figure S35	Docked NCs on Au(111)@SR with higher coverage monolayers	32
Figure S36	Ag NC docking on optimized Au(111)@SR surfaces	33
Table S1	BE of docked Ag <sub>n</sub> (SR) <sub>m</sub> NCs on Au(111) surface with higher thiolate coverage	33
Table S2	BE of docked NCs on Au(111)@SR with different numbers of monolayer staples	34
Table S3	DFT calculated energies of parent NCs and Au and Ag atoms	34
Table S4	Isomers of single gold atom substituted [AuAg <sub>24</sub> (DMBT) <sub>18</sub> ] <sup>-</sup>	34
Table S5	Isomers of double gold-atom substituted [Au <sub>2</sub> Ag <sub>23</sub> (DMBT) <sub>18</sub> ] <sup>-</sup>	35
Figure S37	Doping pathway of Au atom in [Ag <sub>29</sub> (BDT) <sub>12</sub> (TPP) <sub>4</sub> ] <sup>3-</sup> NC	35
Table S6	Energies of isomers of single gold atom substituted [AuAg <sub>28</sub> (BDT) <sub>12</sub> (TPP) <sub>4</sub> ] <sup>3-</sup>	35
Figure S38	Optimized Ag-doped Au(111)@SR surfaces	36
SI 7	Energies of DFT-optimized Au(111)@SR surfaces	36
Table S7	Energies of undoped Au(111) monolayer surfaces	36
Table S8	Energies of Ag-alloy isomers of [Au(111)Ag@(DMBT-Au <sub>ad</sub> -DMBT)] surface with a single Ag atom	36
Table S9	Ag-alloy isomers of the Au(111)Ag@BDT surface	37

Figure S39	Reaction energies for the metallic exchange in Ag NC–Au(111)@SR surface system	37
SI 8	References	38-39

## SI 1. Experimental section

**Instrumentation.** UV-Vis Spectroscopy: The optical absorption spectra were recorded using a Perkin Elmer Lambda 25 instrument with a range of 200 – 1100 nm and a band-pass filter of 1 nm.

**HRTEM:** High-resolution transmission electron microscopic (HRTEM) imaging was carried out on a JEOL 3010, 300 kV instrument with a UHR polepiece. Energy dispersive analysis (EDS) was performed using an Oxford EDAX connected to the HRTEM. A Gatan 794 multiscan CCD camera was used to capture the images. Samples were prepared by dropcasting the dispersion on carbon-coated copper grids (spi Supplies, 3530C-MB) and dried at ambient conditions.

**ESI MS:** All the mass spectrometric measurements were carried out in a Waters Synapt G2-Si instrument. The instrument is well equipped with electrospray ionization, and all spectra were measured in the negative ion and resolution mode. The instrument has the capability of measuring ESI MS with high-resolution up to the orders of 50,000 (m/Dm). NaI was used for calibrating the instrument. The measurement conditions were optimized to a capillary voltage of 3 kV, a cone voltage of 20 V, a desolvation gas flow of 400 L/h, a source temperature of 100 °C, a desolvation temperature of 150°C, and a sample infusion rate of 30 mL/h.

**HAADF-STEM and EDS mapping:** The high-angle annular dark-field scanning transmission electron microscopic imaging was carried out in a JEOL JEM-2800 high-throughput electron microscope equipped with a Schottky-type field emission gun operating at 200 kV with simultaneous bright field (BF) and dark field (DF) STEM imaging modes.

The energy-dispersive X-ray (EDS) spectra and elemental mapping were collected using dual silicon drift detectors.

**Raman spectroscopy:** Raman measurements were carried out using a WITec GmbH alpha300S confocal Raman equipped with a 532 nm laser as the excitation source. Measurements involved a 20× objective (Plan-Apochromat, Zeiss), 600 grooves/mm grating for 1 s acquisition time. A laser power of ~800 μW was maintained on the sample throughout the measurement.

**Materials and methods.** Silver nitrate (AgNO<sub>3</sub>, ≥99%), 2-phenylethanethiol (PET, 98%), 2,4-dimethylbenzenethiol (DMBT, 95%), 1,3-benzenedithiol (BDT, 99%), 4-fluorothiophenol (FTP, 98%), triphenylphosphine (TPP, 99%), tetraoctylammonium bromide (TOABr, 98%) and sodium borohydride (NaBH<sub>4</sub>, ≥99%) were purchased from Sigma Aldrich. Tetrachloroauric acid (HAuCl<sub>4</sub>·3H<sub>2</sub>O) was prepared from pure gold and aqua regia in the laboratory. All the solvents (dichloromethane, hexane, methanol, and toluene) used were of HPLC grade without further purification. Millipore-produced deionized water (~18.2 MΩ) was used throughout the experiments.

**Synthesis of Au@DMBT nanoparticles.** The synthesis of 2,4-dimethylbenzenethiol-capped Au nanoparticles, referred to as Au@DMBT NPs, was carried out using a modified Brust-Schiffrin synthesis method.<sup>1</sup> Initially, an aqueous solution of HAuCl<sub>4</sub>·3H<sub>2</sub>O (5.0 mg in 0.5 mL H<sub>2</sub>O) was mixed with a solution of tetraoctylammonium bromide (TOABr, 13.4 mg) in 30 mL toluene. The aqueous-organic mixture was vigorously stirred for 15 min, and then 7 μL of 2,4-DMBT was added. Next, 2.0 mg of NaBH<sub>4</sub> in 10 mL of ice-cold water was added dropwise with vigorous stirring as the color of the reaction mixture turned purple. After stirring for nearly an hour, the organic layer was separated, and the size focussing was done with overnight heating at 60 °C. The color of the organic layer changed from purple to wine-red. Further purification was performed by removing the solvent under reduced pressure using a rotary evaporator and washing it with ethanol. Finally, the purified NP was extracted in toluene, dried in a rotary evaporator, and stored in a refrigerator.

The synthesized Au@DMBT NPs were characterized using optical absorption spectroscopy and HRTEM, as presented in Figure S1. From the particle size distribution, the NPs were found to have an average size of 4.46 ± 0.64 nm, referred to as ~ 4.5 nm Au@DMBT NPs. Please note that for particle size calculation, we are referring to the most probable diameter of the metallic core of the particle.

**Synthesis of Au@BDT nanoparticles.** 1,3-Benzenedithiol-protected Au NPs, referred to as Au@BDT NPs, were synthesized by modifying the typical Brust-Schiffrin synthesis protocol.<sup>1</sup> In a typical synthesis, an aqueous solution of HAuCl<sub>4</sub>·3H<sub>2</sub>O (15.0 mg in 0.5 mL H<sub>2</sub>O) was mixed with a solution of TOABr (104.0 mg) in 30 mL toluene. The aqueous-organic mixture was vigorously stirred for 15 min, and then 2 μL of 1,3-BDT was added. Next, 13.6 mg of NaBH<sub>4</sub> in 10 mL of ice-cold water was added in a dropwise manner with vigorous stirring as the reaction mixture turned purple. After an hour, the organic layer was separated, and the size focussing was done with overnight heating at 60 °C. With heating, the organic layer turned to wine-red from purple. For purification, the solvent was rotary evaporated, followed by ethanol wash. Finally, the purified NPs were extracted in toluene, dried in a rotary evaporator, and stored in a refrigerator.

The synthesized Au@BDT NPs were characterized using optical absorption spectroscopy and HRTEM; the data are presented in Figure S11. From the particle size distribution, the NPs were found to have an average size of 3.70 ± 0.48 nm, referred to as ~ 3.7 nm Au@DMBT NPs. Please note, for particle size calculation, we are referring to the most probable diameter of the metallic core of the particle.

**Synthesis of [Ag<sub>25</sub>(DMBT)<sub>18</sub>]<sup>-</sup> nanocluster.** The NC was synthesized by slightly modifying a previously reported protocol.<sup>2</sup> First, 38.0 mg of AgNO<sub>3</sub> was dissolved in 2 mL of methanol. To this mixture, 90 μL of 2,4-DMBT was added, which produced an insoluble yellow Ag-thiolate, followed by 17 mL of DCM, and then it was stirred for 15 mins at 0 °C. Afterwards, 0.5 mL of methanolic solution of 6 mg PPh<sub>4</sub>Br was added, followed by dropwise addition of 15.0 mg of NaBH<sub>4</sub> in 0.5 mL of ice-cold water. The reaction mixture was further stirred for 7-8 h, followed by overnight aging in the refrigerator. For purification, the crude cluster solution was centrifuged to remove any insoluble impurities, and the collected supernatant was concentrated by rotary evaporation. The precipitate was washed multiple times with methanol. Then, the nanocluster was extracted in DCM and centrifuged again to remove any remaining insoluble impurities. DCM was removed using rotavapor, and the purified NC was obtained in its powdered form.

The purified NC was characterized using optical absorption microscopy, HRTEM, and ESI MS (Figure S2).

**Synthesis of [Ag<sub>29</sub>(BDT)<sub>12</sub>(TPP)<sub>4</sub>]<sup>3-</sup> nanocluster.** The NC was synthesized following a reported method with a slight modification.<sup>3</sup> Briefly, 20.0 mg of AgNO<sub>3</sub> was dissolved in a

solvent mixture of 2 mL methanol and 10 mL DCM. To this mixture, 13.5  $\mu\text{L}$  of 1,3-BDT was added and stirred for 15 min. Then, an aqueous solution of 10.5 mg  $\text{NaBH}_4$  in 0.5 mL ice-cold water was added dropwise and stirred for another 5 h in dark. Next, the reaction mixture was centrifuged to eliminate insoluble impurities, and the crude cluster was obtained as an orange supernatant. The supernatant was concentrated by rotary evaporation, and the precipitate was washed with methanol. Finally, the purified NC was extracted in DMF.

Optical absorption microscopy, HRTEM, and ESI MS characterization of purified NC solution in DMF confirmed the formation of  $[\text{Ag}_{29}(\text{BDT})_{12}(\text{TPP})_4]^{3-}$  (Figure S13).

**Synthesis of  $[\text{PPh}_4]_n[\text{Ag}_{44}(\text{FTP})_{30}]$  nanocluster.** The NC was prepared following a solid-state synthetic route.<sup>4</sup> In a typical synthesis, 20.0 mg of  $\text{AgNO}_3$  and 12.0 mg of  $\text{PPh}_4\text{Br}$  were thoroughly grounded in an agate mortar and pestle for 5 min. Next, 76  $\mu\text{L}$  of 4-FTP was added to the reaction mixture in one shot and further grounded for three more minutes. In the next step, 45.0 mg of  $\text{NaBH}_4$  was added and ground until the mixture turned into a brown paste. The mixture was extracted using 7 mL of DCM and left undisturbed at room temperature till the optical absorption spectra showed all the characteristic features of the NC. For the purification, the NC was precipitated with hexane and collected by centrifugation. The precipitate was washed multiple times with hexane, dissolved in DCM, and centrifuged to remove any thiolate impurities. Finally, the purified NC solution was vacuum-dried and stored in the refrigerator. Optical absorption microscopy, HRTEM, and ESI MS characterization of purified NC solution in DCM confirmed the formation of  $\text{Ag}_{44}(\text{FTP})_{30}$  (Figure S18).  $[\text{Ag}_{44}(\text{FTP})_{30}]^{3-}$  and  $[\text{Ag}_{44}(\text{FTP})_{30}]^{4-}$  were the prominent features in the MS of the pure  $\text{Ag}_{44}(\text{FTP})_{30}$  NC (Figure S18A).

## SI 2. Concentration calculation

### (a) $[\text{Ag}_{25}(\text{DMBT})_{18}]^-$ NCs

Molecular weight = 5167

$$\text{Mass of a } [\text{Ag}_{25}(\text{DMBT})_{18}]^- \text{ NC, } m = \frac{5167 \times 10^3}{6.023 \times 10^{23}} = 8.58 \times 10^{-18} \text{ mg}$$

$$\text{Mass of } [\text{Ag}_{25}(\text{DMBT})_{18}]^- \text{ NCs in the stock solution, } W = 1 \frac{\text{mg}}{10 \text{ mL}} = 0.1 \times 10^3 \frac{\text{mg}}{\text{L}}$$

$$\text{Number of particles in the sample, } N = \frac{W}{m} = \frac{0.1 \times 10^3}{8.58 \times 10^{-18}} = 1.16 \times 10^{19} \frac{\text{particles}}{\text{L}}$$

$$\text{Molarity of Au@DMBT NPs in solution, } M_1 = \frac{N}{N_A} = \frac{1.16 \times 10^{19}}{6.023 \times 10^{23}} \text{ M} = 19.3 \mu\text{M}$$

For interparticle reaction (reaction@NP),

0.3 mL ( $V_1$ ) of  $\text{Ag}_{25}$  NC from the above solution is diluted to make a 3.3 mL ( $V_2$ ) solution.

Using the formula,  $M_1V_1 = M_2V_2$

$$\text{Molarity of } [\text{Ag}_{25}(\text{DMBT})_{18}]^- \text{ NC, } M_2 = \frac{19.3 \mu\text{M} \times 0.3 \text{ mL}}{3.3 \text{ mL}} = 1.75 \mu\text{M}$$

For ESI MS measurements (reaction@NC),

1 mL ( $V_1$ ) of  $[\text{Ag}_{25}(\text{DMBT})_{18}]^-$  NC from the above solution is diluted to make a 6 mL ( $V_2$ ) solution.

Using the formula,  $M_1V_1 = M_2V_2$

$$\text{Molarity of } [\text{Ag}_{25}(\text{DMBT})_{18}]^- \text{ NC, } M_2 = \frac{19.3 \mu\text{M} \times 1 \text{ mL}}{6 \text{ mL}} = 3.22 \mu\text{M}$$

Size of the metal core of the  $[\text{Ag}_{25}(\text{DMBT})_{18}]^-$  NC (from the single crystal XRD) =  $\sim 1$  nm; please note that the metal core diameter as measured in HRTEM (1.9 nm) is slightly overestimated.

$$\text{Surface area of a } \text{Ag}_{25} \text{ NC} = 4\pi R^2 = 3.14 \text{ nm}^2$$

A  $[\text{Ag}_{25}(\text{DMBT})_{18}]^-$  NC surface is covered by 18 DMBT ligands.

So, let's assume a DMBT ligand occupies a surface area of  $0.17 \text{ nm}^2$ .

$$\text{Mass of 1 DMBT (C}_8\text{H}_9\text{S) ligand, } m_{\text{DMBT}} = \frac{137.23 \times 10^3}{6.023 \times 10^{23}} \text{ mg} = 2.28 \times 10^{-19} \text{ mg}$$

### (b) Au@DMBT NPs

Average size of Au NP (metal core from HRTEM),  $2R = 4.5 \text{ nm}$

$$\text{Volume of a Au NP (sphere), } V = \frac{4}{3}\pi R^3 = 47.69 \text{ nm}^3$$

Let us consider that Au NPs have an fcc structure with a packing fraction of 74%.

$$\text{Net volume of a Au NP, } V_{\text{NP}} = 74\% \text{ of } V = 35.29 \text{ nm}^3$$

Radius of a Au atom,  $R_{\text{Au}} = 0.146 \text{ nm}$

$$\text{Volume of a Au atom (sphere), } V_{\text{Au}} = \frac{4}{3}\pi R_{\text{Au}}^3 = 0.013 \text{ nm}^3$$

$$\text{Number of Au atoms per NP, } N_{\text{Au}} = \frac{V_{\text{NP}}}{V_{\text{Au}}} = \sim 2715$$

Mass of a Au atom,  $m_{\text{Au}} = 196.96 \text{ u}$

$$\text{Mass of the metal core, } m_{\text{core}} = \frac{N_{\text{Au}} \times m_{\text{Au}}}{N_A} = \frac{2715 \times 196.96 \times 10^3}{6.023 \times 10^{23}} \text{ mg} = 8.88 \times 10^{-16} \text{ mg}$$

The exact ligand coverage over the plasmonic Au NPs is not known. From our calculations on 2,4-DMBT ligand coverage on a  $[\text{Ag}_{25}(\text{DMBT})_{18}]^-$  NC, we are approximating that 1 DMBT ligand occupies a surface area of  $\sim 0.17 \text{ nm}^2$  on a Au NP surface. However, the ligand packing is likely to differ from our approximation.

$$\text{Surface area of Au NP} = 4\pi R^2 = 63.58 \text{ nm}^2$$

$$\text{Number of DMBT ligands per NP, } N_{\text{DMBT}} = \sim 374$$

$$\text{Mass of total ligand coverage, } m_{\text{ligand}} = N_{\text{DMBT}} \times m_{\text{DMBT}} = 8.52 \times 10^{-17} \text{ mg}$$

$$\text{Total mass of a Au@DMBT NP, } m = m_{\text{core}} + m_{\text{ligand}} = 9.73 \times 10^{-16} \text{ mg}$$

For interparticle reaction (reaction@NP),

$$\text{Weight of Au NP (dry weight of the sample), } W = 5 \frac{\text{mg}}{3.3 \text{ mL}} = 1.51 \times 10^3 \frac{\text{mg}}{\text{L}}$$

$$\text{Number of particles in the sample, } N = \frac{W}{m} = \frac{1.51 \times 10^3}{9.73 \times 10^{-16}} = 1.55 \times 10^{18} \frac{\text{particles}}{\text{L}}$$

$$\text{Molarity of Au@DMBT NPs in solution, } M_1 = \frac{N}{N_A} = \frac{1.55 \times 10^{18}}{6.023 \times 10^{23}} \text{ M} = 2.5 \mu\text{M}$$

For ESI MS measurements (reaction@NC),

0.3 mL ( $V_1$ ) of Au NP from the above solution is further diluted to make a 6 mL ( $V_2$ ) solution.

Using the formula,  $M_1 V_1 = M_2 V_2$

$$\text{Particle molarity of Au@DMBT NPs, } M_2 = \frac{2.5 \mu\text{M} \times 0.3 \text{ mL}}{6 \text{ mL}} = 0.12 \mu\text{M}$$

### (c) $[\text{Ag}_{29}(\text{BDT})_{12}(\text{TPP})_4]^{3-}$ NCs

Molecular weight = 5857

$$\text{Mass of a } [\text{Ag}_{29}(\text{BDT})_{12}(\text{TPP})_4]^{3-} \text{ NC, } m = \frac{5857 \times 10^3}{6.023 \times 10^{23}} = 9.72 \times 10^{-18} \text{ mg}$$

$$\text{Mass of } [\text{Ag}_{29}(\text{BDT})_{12}(\text{TPP})_4]^{3-} \text{ NCs in the stock solution, } W = 1 \frac{\text{mg}}{10 \text{ mL}} = 0.1 \times 10^3 \frac{\text{mg}}{\text{L}}$$

$$\text{Number of particles in the sample, } N = \frac{W}{m} = \frac{0.1 \times 10^3}{9.72 \times 10^{-18}} = 1.03 \times 10^{19} \frac{\text{particles}}{\text{L}}$$

$$\text{Molarity of Au@BDT NPs in solution, } M_1 = \frac{N}{N_A} = \frac{1.03 \times 10^{19}}{6.023 \times 10^{23}} \text{ M} = 17.1 \mu\text{M}$$

For interparticle reaction (reaction@NP),

0.3 mL ( $V_1$ ) of  $[\text{Ag}_{29}(\text{BDT})_{12}(\text{TPP})_4]^{3-}$  NC from the above solution is diluted to make a 3.3 mL ( $V_2$ ) solution.

Using the formula,  $M_1 V_1 = M_2 V_2$

$$\text{Molarity of } [\text{Ag}_{29}(\text{BDT})_{12}(\text{TPP})_4]^{3-} \text{ NC, } M_2 = \frac{17.1 \mu\text{M} \times 0.3 \text{ mL}}{3.3 \text{ mL}} = 1.55 \mu\text{M}$$

For ESI MS measurements (reaction@NC),

1 mL ( $V_1$ ) of  $[\text{Ag}_{29}(\text{BDT})_{12}(\text{TPP})_4]^{3-}$  NC from the above solution is diluted to make a 6 mL ( $V_2$ ) solution.

Using the formula,  $M_1V_1 = M_2V_2$

$$\text{Molarity of } [\text{Ag}_{29}(\text{BDT})_{12}(\text{TPP})_4]^{3-} \text{ NC, } M_2 = \frac{17.1 \mu\text{M} \times 1 \text{ mL}}{6 \text{ mL}} = 2.85 \mu\text{M}$$

Size of the metal core of the  $[\text{Ag}_{29}(\text{BDT})_{12}(\text{TPP})_4]^{3-}$  NC (from the single crystal XRD) =  $\sim 1$  nm; please note that the metal core diameter as measured in HRTEM (1.7 nm) is slightly overestimated.

$$\text{Surface area of a } [\text{Ag}_{29}(\text{BDT})_{12}(\text{TPP})_4]^{3-} \text{ NC} = 4\pi R^2 = 3.14 \text{ nm}^2$$

A  $[\text{Ag}_{29}(\text{BDT})_{12}(\text{TPP})_4]^{3-}$  NC surface is covered by 12 BDT and 4 TPP ligands.

Let's assume that the bidentate and monodentate ligands, i.e, BDT and TPP, contribute 85.7% and 14.3% of the total ligand shell, respectively.

So, 1 BDT ligand occupies a surface area of  $0.22 \text{ nm}^2$ .

$$\text{Mass of 1 BDT (C}_6\text{H}_4\text{S}_2\text{) ligand, } m_{\text{BDT}} = \frac{140.24 \times 10^3}{6.023 \times 10^{23}} \text{ mg} = 2.32 \times 10^{-19} \text{ mg}$$

#### (d) Au@BDT NP

Average size of Au NP (metal core from HRTEM),  $2R = 3.7 \text{ nm}$

$$\text{Volume of a Au NP (sphere), } V = \frac{4}{3}\pi R^3 = 26.51 \text{ nm}^3$$

Let us consider that Au NPs have an fcc structure with a packing fraction of 74%.

$$\text{Net volume of a Au NP, } V_{\text{NP}} = 74\% \text{ of } V = 19.62 \text{ nm}^3$$

Radius of a Au atom,  $R_{\text{Au}} = 0.146 \text{ nm}$

$$\text{Volume of a Au atom (sphere), } V_{\text{Au}} = \frac{4}{3}\pi R_{\text{Au}}^3 = 0.013 \text{ nm}^3$$

$$\text{Number of Au atoms per NP, } N_{\text{Au}} = \frac{V_{\text{NP}}}{V_{\text{Au}}} = \sim 1509$$

Mass of a Au atom,  $m_{\text{Au}} = 196.96 \text{ u}$

$$\text{Mass of the metal core, } m_{\text{core}} = \frac{N_{\text{Au}} \times m_{\text{Au}}}{N_{\text{A}}} = \frac{1509 \times 196.96 \times 10^3}{6.023 \times 10^{23}} \text{ mg} = 4.93 \times 10^{-16} \text{ mg}$$

The exact ligand coverage over the plasmonic Au NPs is not known. From our calculations on 1,3-BDT ligand coverage on a  $[\text{Ag}_{29}(\text{BDT})_{12}(\text{TPP})_4]^{3-}$  NC, we are approximating that 1 BDT ligand occupies a surface area of  $\sim 0.22 \text{ nm}^2$  on a Au NP surface. However, the ligand packing is likely to differ from our approximation.

$$\text{Surface area of Au NP} = 4\pi R^2 = 42.99 \text{ nm}^2$$

Number of BDT ligands per NP,  $N_{\text{DMBT}} = \sim 195$

Mass of total ligand coverage,  $m_{\text{ligand}} = N_{\text{DMBT}} \times m_{\text{DMBT}} = 4.52 \times 10^{-17} \text{ mg}$

Total mass of a Au@BDT NP,  $m = m_{\text{core}} + m_{\text{ligand}} = 5.38 \times 10^{-16} \text{ mg}$

For interparticle reaction (reaction@NP),

Weight of Au NP (dry weight of the sample),  $W = 5 \frac{\text{mg}}{3.3 \text{ mL}} = 1.51 \times 10^3 \frac{\text{mg}}{\text{L}}$

Number of particles in the sample,  $N = \frac{W}{m} = \frac{1.51 \times 10^3}{5.38 \times 10^{-16}} = 2.81 \times 10^{18} \frac{\text{particles}}{\text{L}}$

Molarity of Au@BDT NPs in solution,  $M_1 = \frac{N}{N_A} = \frac{2.81 \times 10^{18}}{6.023 \times 10^{23}} \text{ M} = 4.6 \text{ } \mu\text{M}$

For ESI MS measurements (reaction@NC),

0.3 mL ( $V_1$ ) of Au NP from the above solution is further diluted to make a 6 mL ( $V_2$ ) solution.

Using the formula,  $M_1 V_1 = M_2 V_2$

Molarity of Au@BDT NPs,  $M_2 = \frac{4.6 \text{ } \mu\text{M} \times 0.3 \text{ mL}}{6 \text{ mL}} = 0.23 \text{ } \mu\text{M}$

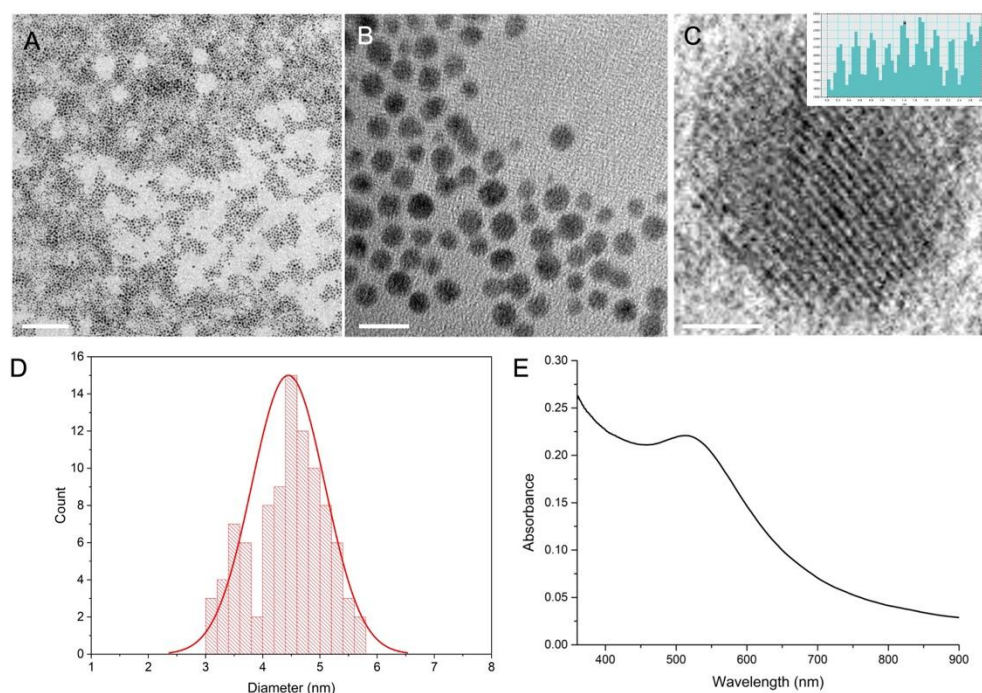


**Figure S1.** Characterization of Au@DMBT NPs. HRTEM images of Au@DMBT NPs captured at different magnifications (A) 0.1  $\mu\text{m}$ , (B) 10, and (C) 2 nm. Profile of inverse fast Fourier transform (IFFT) in the inset of (C). Corresponding particle size distribution (D), and the optical absorption spectrum (E).

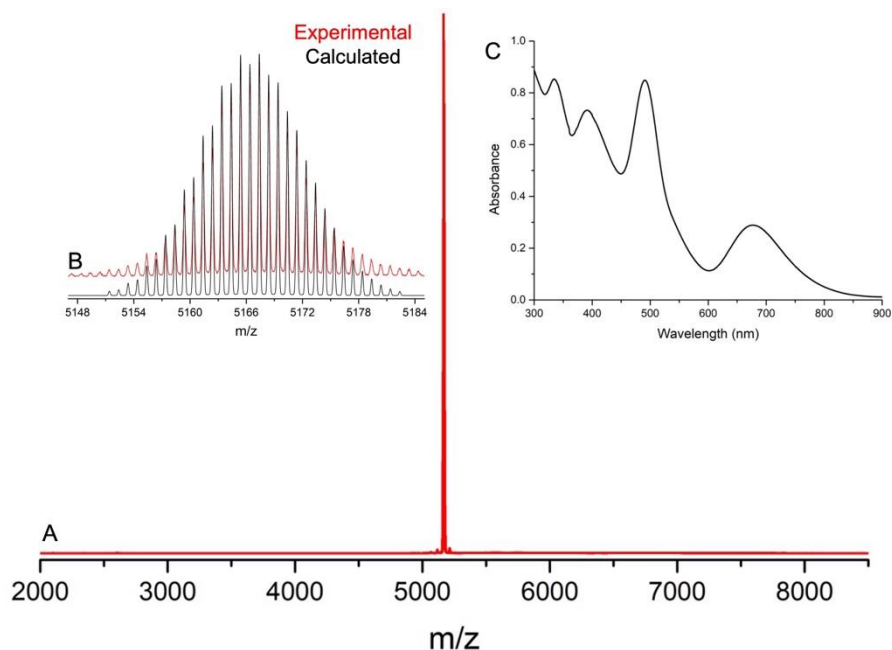


**Figure S2.** Characterization of  $[\text{Ag}_{25}(\text{DMBT})_{18}]^{-}$  NC. (A) ESI MS of the pure NC, (B) comparison of experimental and calculated isotopic distribution pattern, and (C) the optical absorption spectrum. Experimental and calculated spectra are in the red and black trace, respectively.

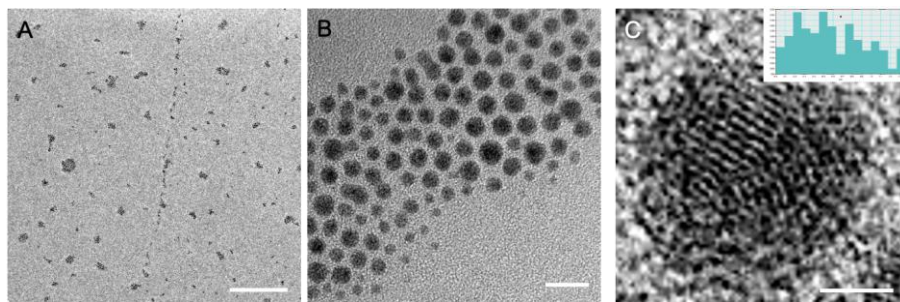


**Figure S3.** HRTEM images of Au@DMBT NPs after reaction with  $[\text{Ag}_{25}(\text{DMBT})_{18}]^{-}$  NC captured at different magnifications (A) 0.2  $\mu\text{m}$ , (B) 10, and (C) 2 nm. Profile of inverse fast Fourier transform (IFFT) in the inset of (C).

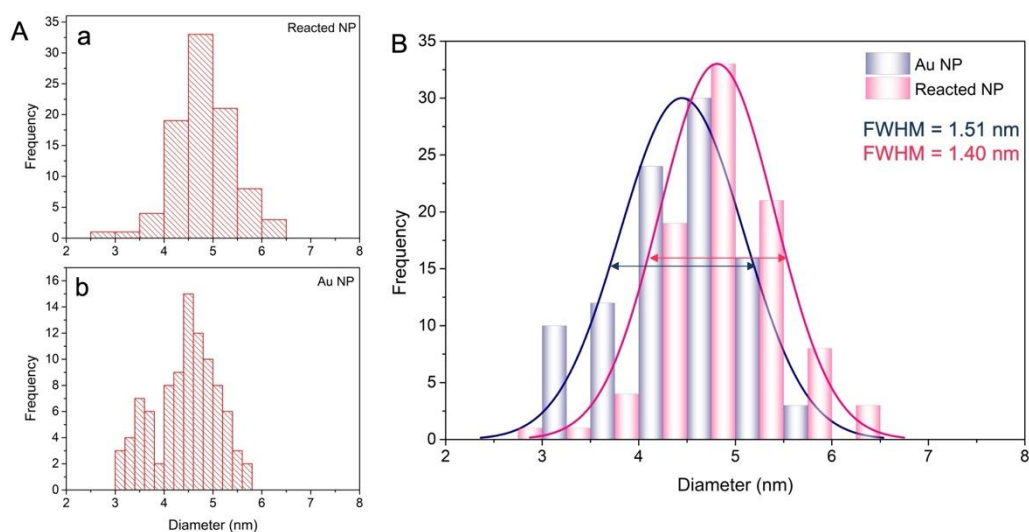


**Figure S4.** Particle size distribution of Au@DMBT NPs plotted as (A) histogram before (a) and after (b) the reaction. (B) Gaussian fitting of the histograms for fwhm calculation.

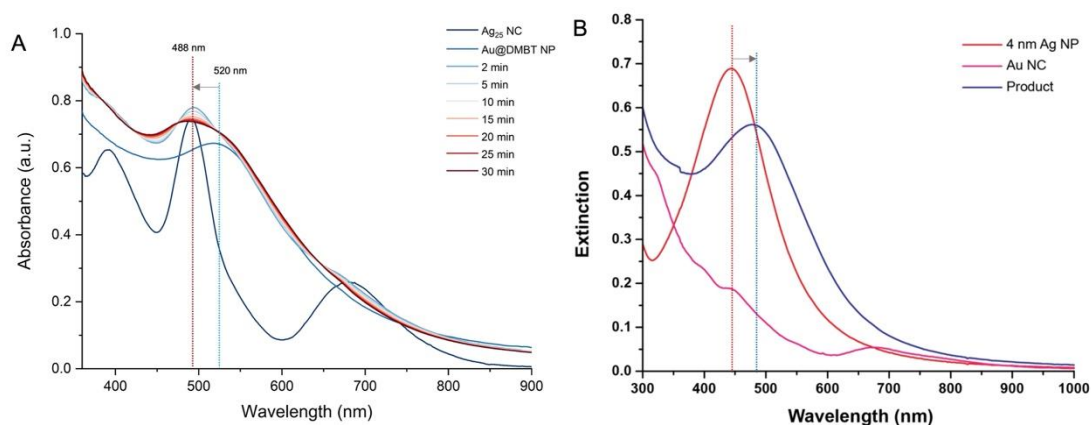


**Figure S5.** Time-dependent optical absorption spectra of the reaction@NP for Au@DMBT NP and  $[Ag_{25}(DMBT)_{18}]^-$  NC system (A). and (B) Optical absorption spectra of the Ag@PET NPs,  $[Au_{25}(PET)_{18}]^-$  NC, and the doped AgAu@PET NP. The doped NP shows a clear red-shifted SPR, a characteristic feature of bimetallic Au-Ag NPs.<sup>5</sup> Copyright 2020 Royal Society Publishing Group.

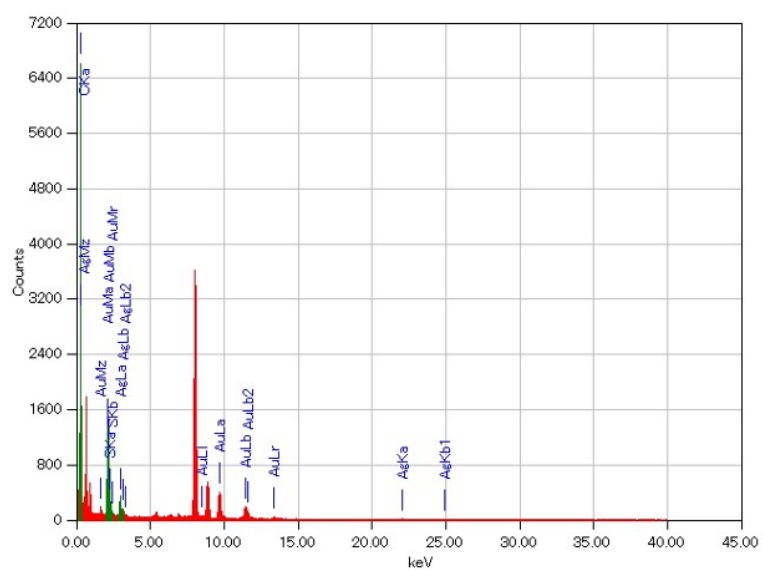


**Figure S6.** EDS spectrum of Au@DMBT and  $[Ag_{25}(DMBT)_{18}]^{-}$  reaction product.

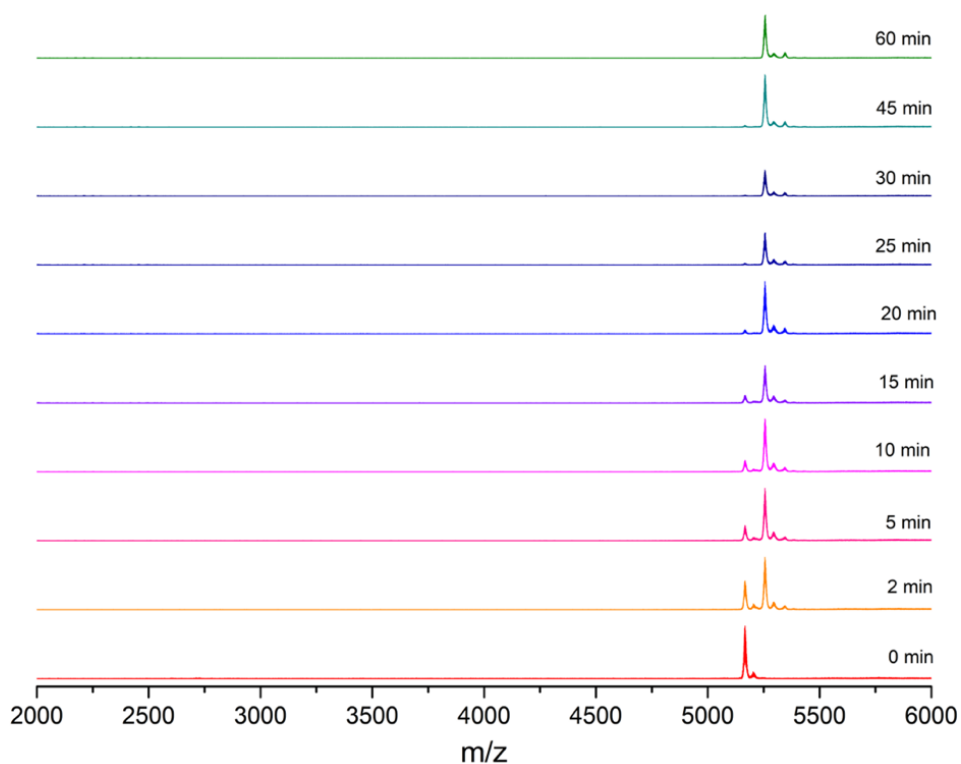


**Figure S7.** Full-range ESI mass spectra of the DMBT-capped-NP and NC reaction.

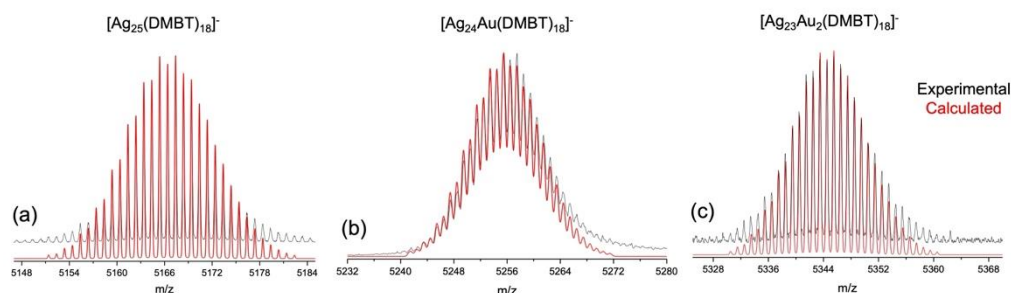


**Figure S8.** Isotopic distribution pattern for the species detected in the ESI MS experiment for the DMBT-capped NP and NC reaction. Experimental and calculated spectra are in the black and red trace, respectively.

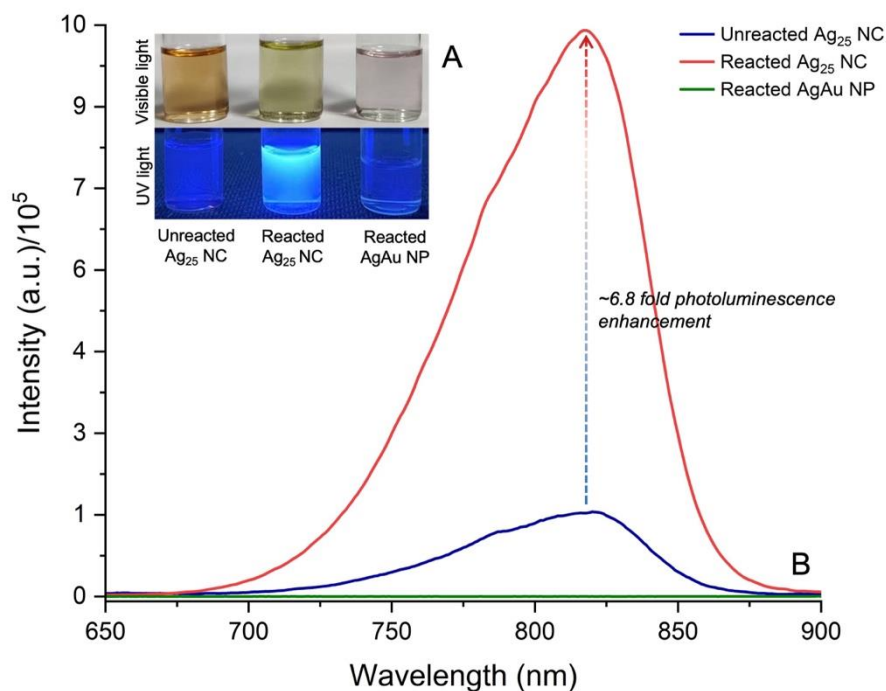


**Figure S9.** Solutions of  $[\text{Ag}_{25}(\text{DMBT})_{18}]^-$  NC, photographed under visible and UV light (A) and their corresponding photoluminescence spectra (B), before and after their reaction with Au@DMBT NP, alongside reacted plasmonic AgAu@DMBT NP.

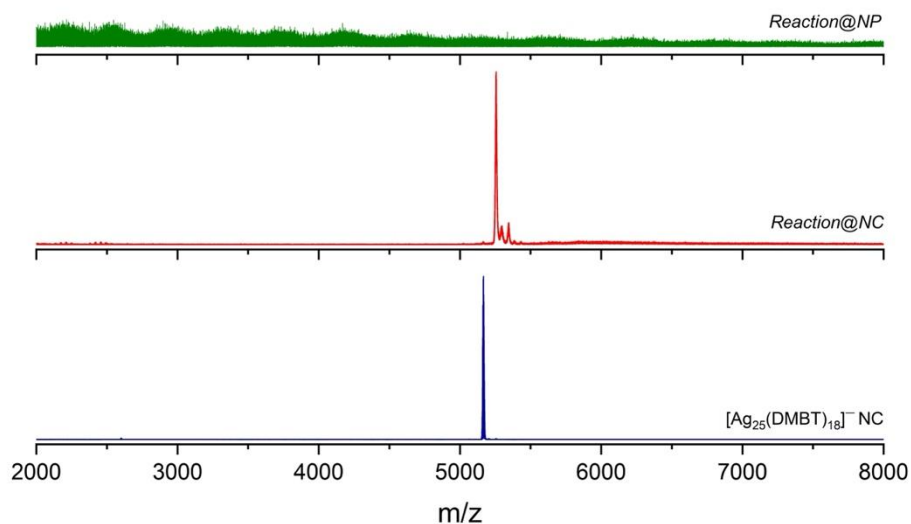


**Figure S10.** A comparative ESI MS of pure  $[\text{Ag}_{25}(\text{DMBT})_{18}]^{-}$  NC and reaction mixture measured after 30 min of reaction@NC and reaction@NP.

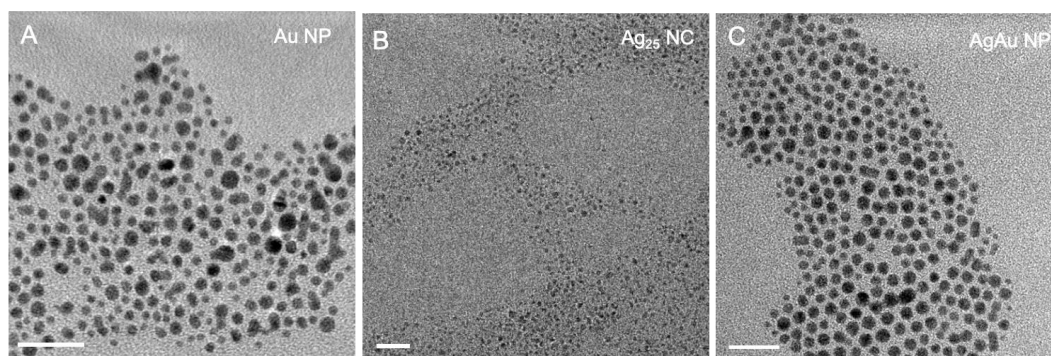


**Figure S11.** Morphological correlation between reactants and the product. TEM images of reactants, Au@DMBT NP (A) and  $[\text{Ag}_{25}(\text{DMBT})_{18}]^{-}$  NC (B), and the product, AgAu@DMBT NP (C). Scale bar: 20 nm.

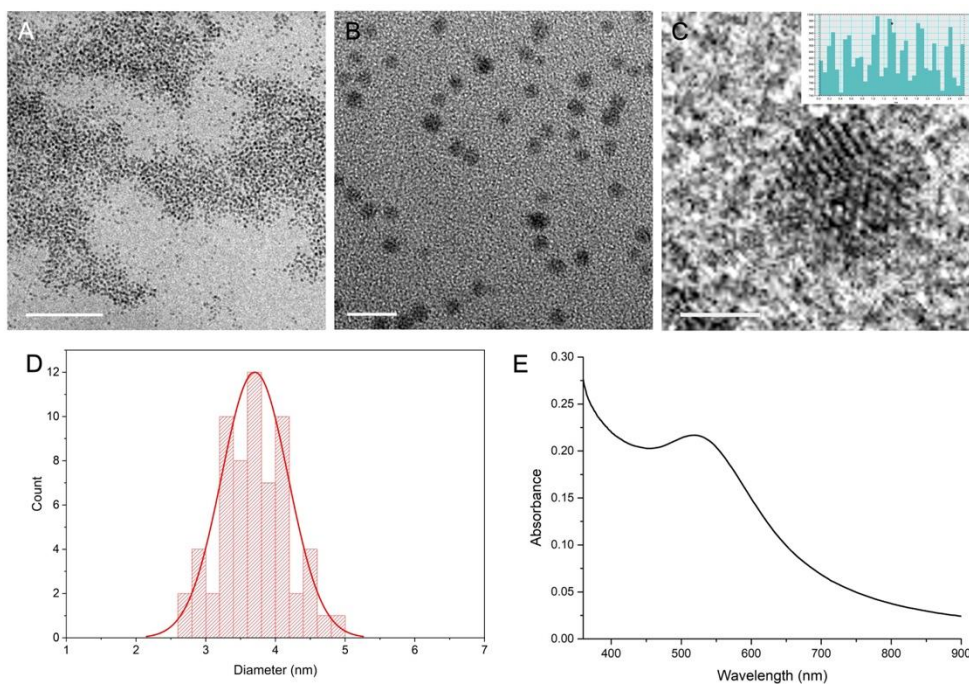


**Figure S12.** Characterization of Au@BDT NPs. HRTEM images of Au@BDT NPs captured at different magnifications (A) 0.1  $\mu\text{m}$ , (B) 10, and (C) 2 nm. Profile of inverse fast Fourier transform (IFFT) in the inset of (C). Corresponding particle size distribution (D), and the optical absorption spectrum (E).

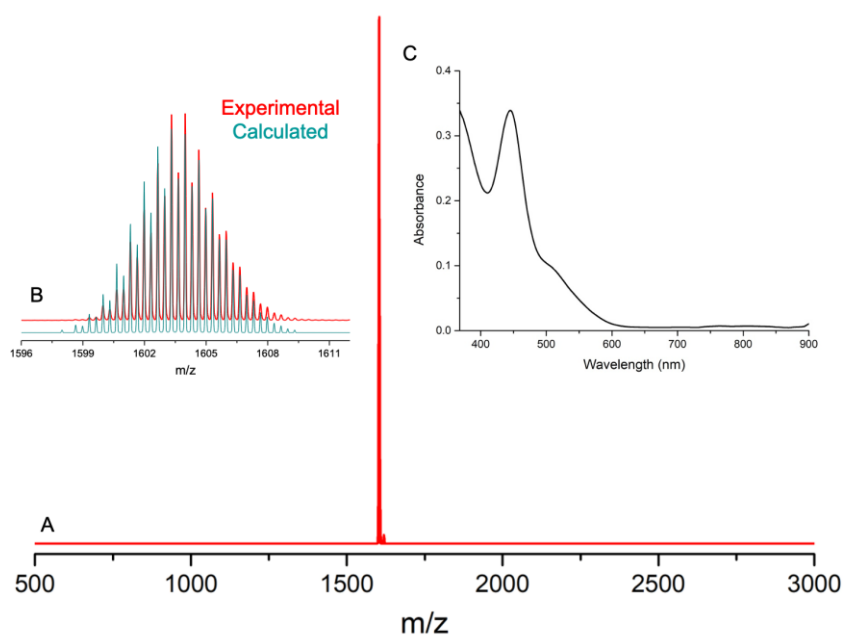


**Figure S13.** Characterization of  $[\text{Ag}_{29}(\text{BDT})_{12}(\text{TPP})_4]^{3-}$  NC. (A) ESI MS of the pure NC after losing 4 TPP ligands, (B) comparison of experimental and calculated isotopic distribution pattern, and (C) the optical absorption spectrum.

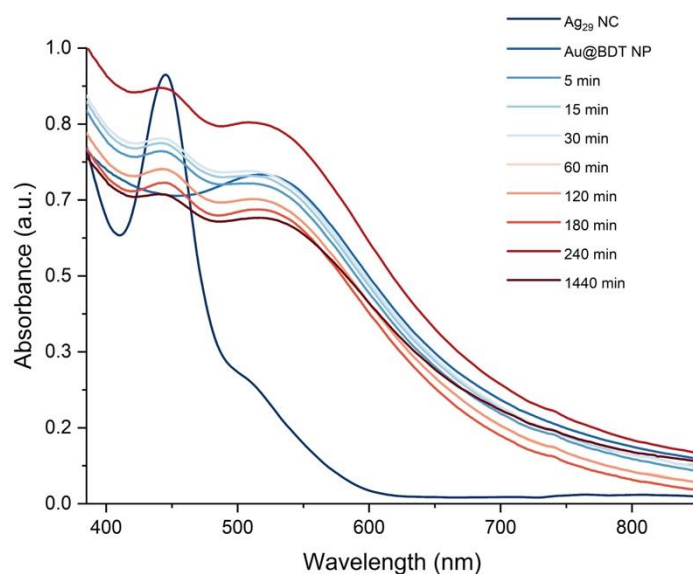


**Figure S14.** Time-dependent optical absorption spectra of the reaction@NP for Au@BDT NP and  $[\text{Ag}_{29}(\text{BDT})_{12}(\text{TPP})_4]^{3-}$  NC reaction. The temporal rise in absorbance is presumably due to aggregation facilitated by non-reactive interparticle interaction, as seen in TEM (Figure S15).

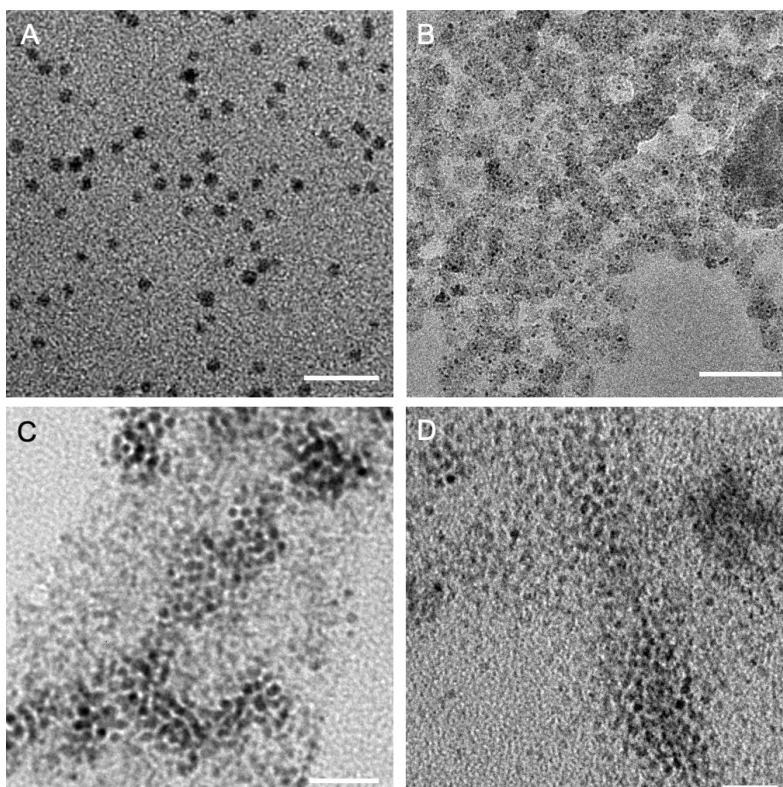


**Figure S15.** TEM image of the starting materials, (A) Au@BDT NP and (B)  $[\text{Ag}_{29}(\text{BDT})_{12}(\text{TPP})_4]^{3-}$  NC, and the reaction mixture imaged after (C) 30 min and (D) 24 h of mixing. For better contrast and to avoid beam-induced damage, the NC was imaged at a lower magnification. Scale bar: (A, C, D) 20, and (B) 100 nm.

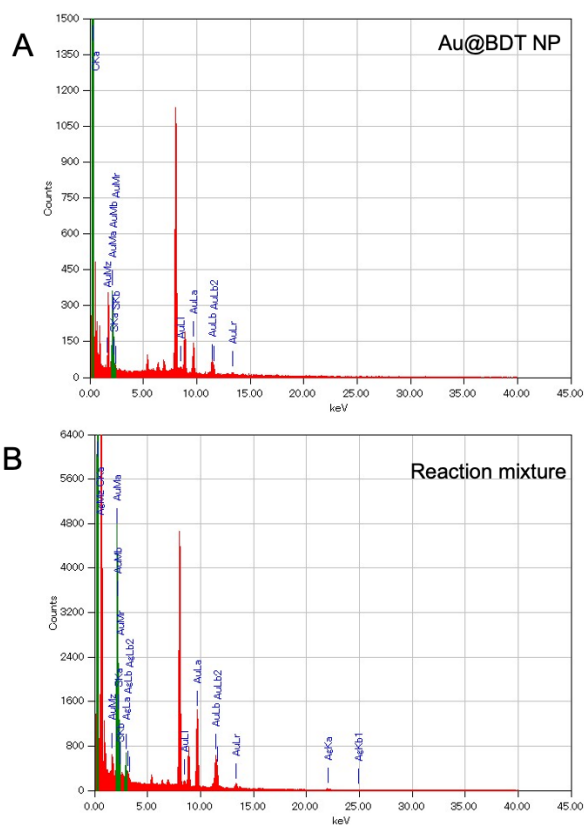


**Figure S16.** EDS spectra showing the elemental composition of Au@BDT NP (A) before, (B) after mixing with  $[\text{Ag}_{29}(\text{BDT})_{12}(\text{TPP})_4]^{3-}$  NC.

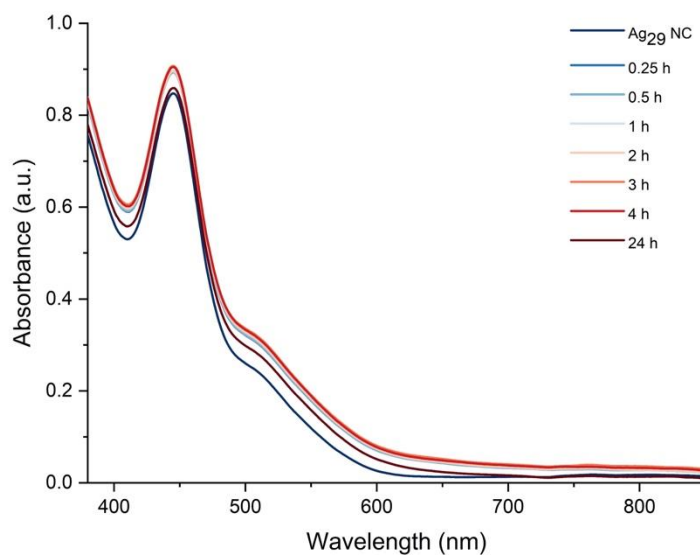


**Figure S17.** Time-dependent optical absorption spectra of the reaction@NC for Au@BDT NP and  $[\text{Ag}_{29}(\text{BDT})_{12}(\text{TPP})_4]^{3-}$  NC system.

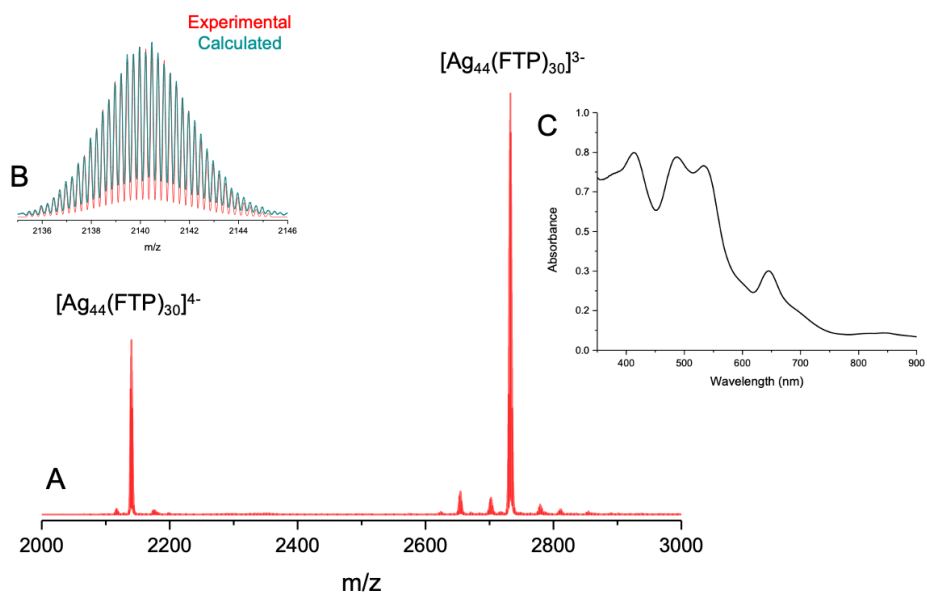


**Figure S18.** Characterization of pure  $[PPh_4]_n[Ag_{44}(FTP)_{30}]$  NC. (A) ESI MS of the pure NC, (B) comparison of experimental and calculated isotopic distribution pattern, and (C) the optical absorption spectrum.

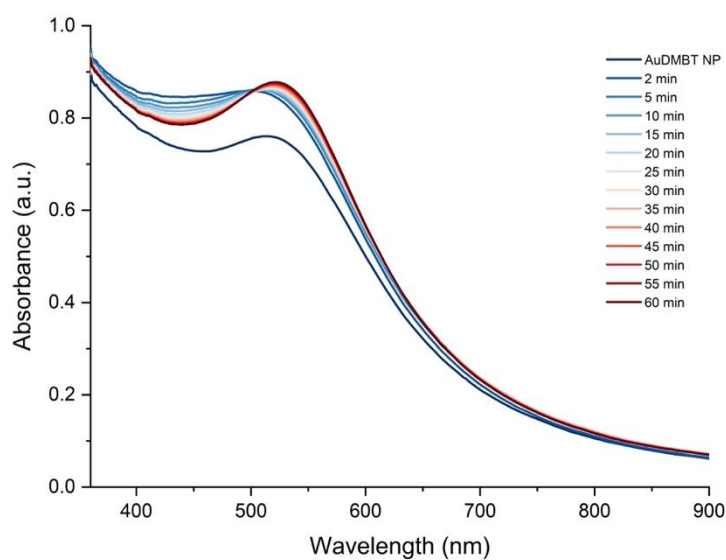


**Figure S19.** Time-dependent optical absorption spectra of the reaction@NP for Au@DMBT NP and  $[Ag_{44}(FTP)_{30}]^{4-}$  NC system.

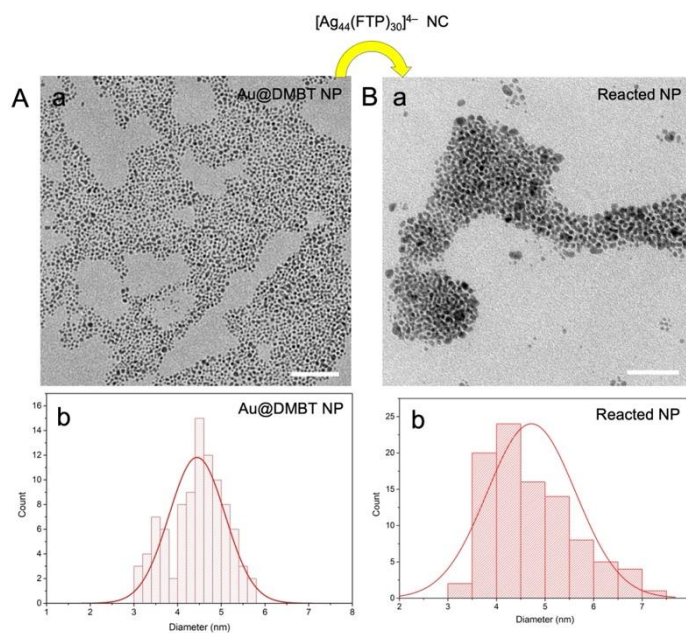


**Figure S20.** Characterization of reaction@NP for Au@DMBT NP and  $[Ag_{44}(FTP)_{30}]^{4-}$  NC system. TEM images (panel-a) and the corresponding particle size distribution (panel-b) of the Au@BDT NPs (A) before and (B) after the reaction. Scale bar: 50 nm.

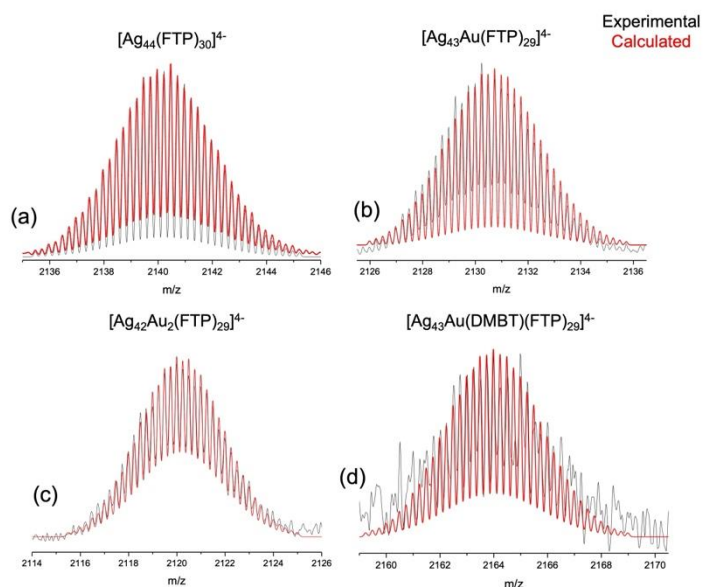


**Figure S21.** Isotopic distribution pattern for the species detected in the ESI MS experiment for the reaction between Au@DMBT NP and  $[Ag_{44}(FTP)_{30}]^{4-}$  NC.

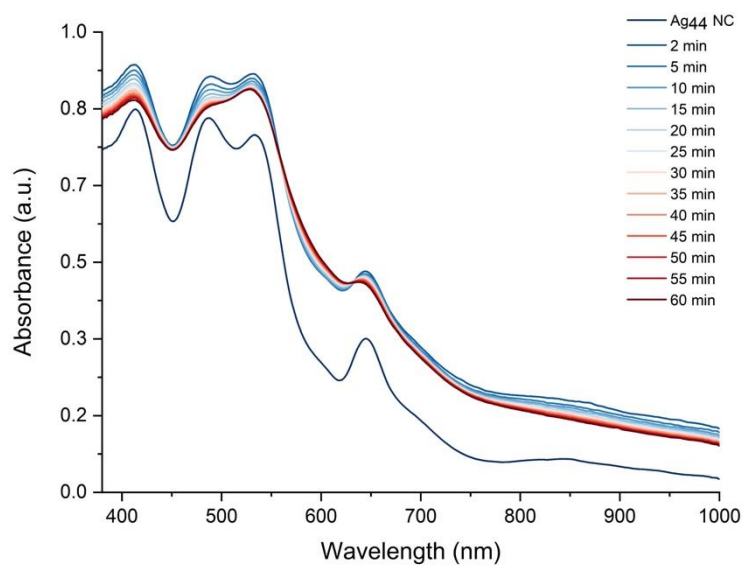


**Figure S22.** Time-dependent optical absorption spectra of the reaction@NC for Au@DMBT NP and  $[Ag_{44}(FTP)_{30}]^{4-}$  NC system.

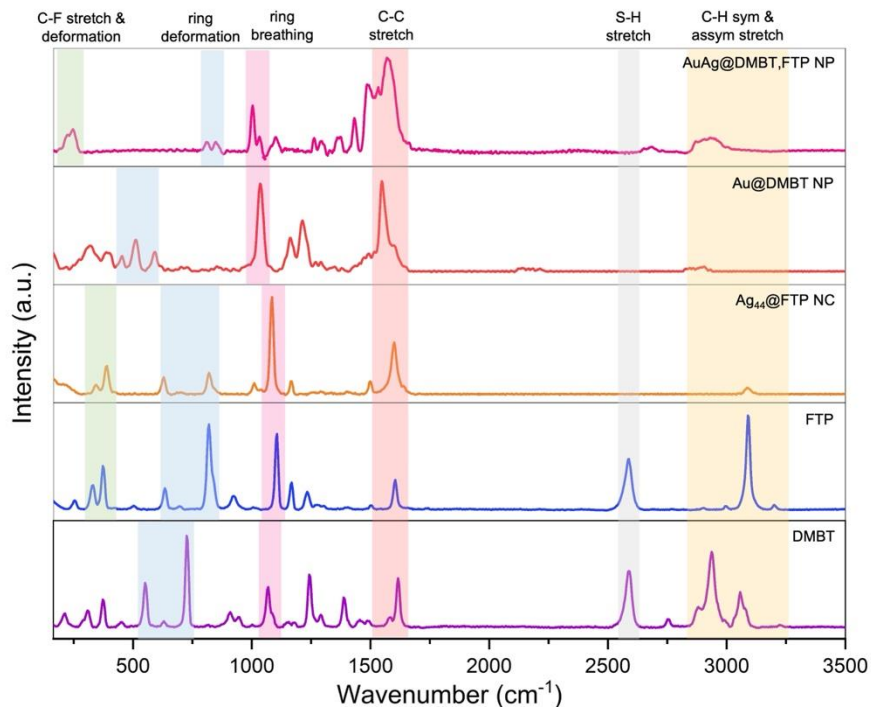


**Figure S23.** Raman spectra of reacted Au NPs were compared to reactants (Au@DMBT NPs and  $[Ag_{44}(FTP)_{30}]^{4-}$  NC) and referenced with exchanging ligands (4-FTP and 2,4-DMBT).

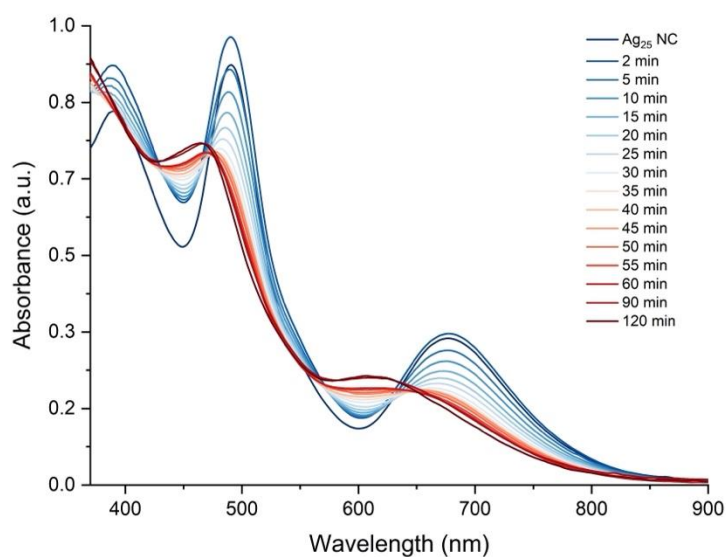


**Figure S24.** Time-dependent optical absorption spectra of the reaction@NC for Au@BDT NP and  $[\text{Ag}_{25}(\text{DMBT})_{18}]^{-}$  NC system.

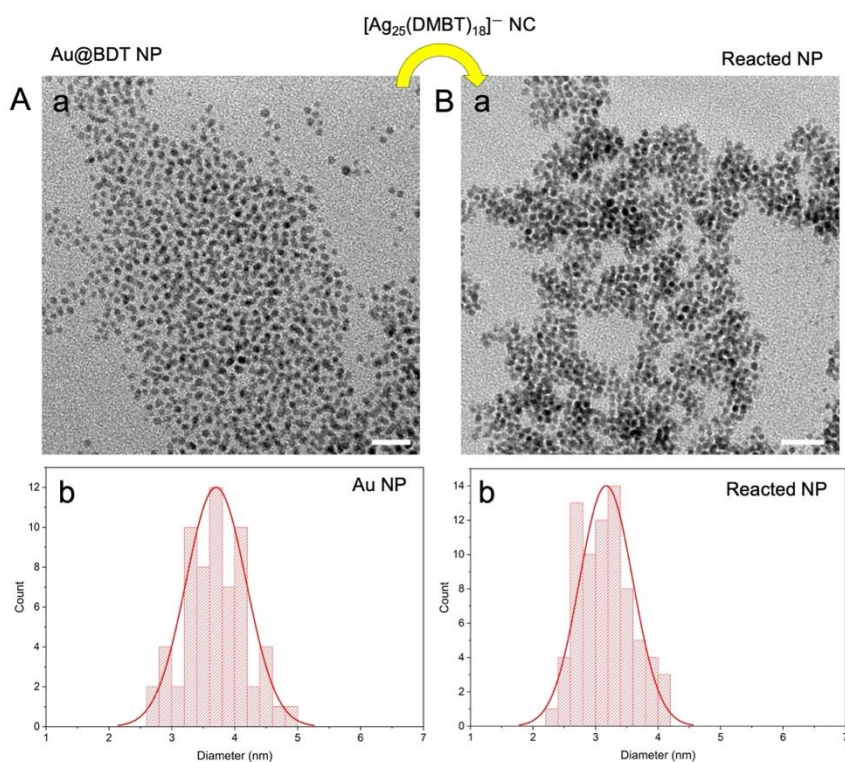


**Figure S25.** Characterization of reaction@NP for Au@BDT NP and  $[\text{Ag}_{25}(\text{DMBT})_{18}]^{-}$  NC system. TEM images (panel-a) and the corresponding particle size distribution (panel-b) of the Au@BDT NPs (A) before and (B) after the reaction. Scale bar: 20 nm.

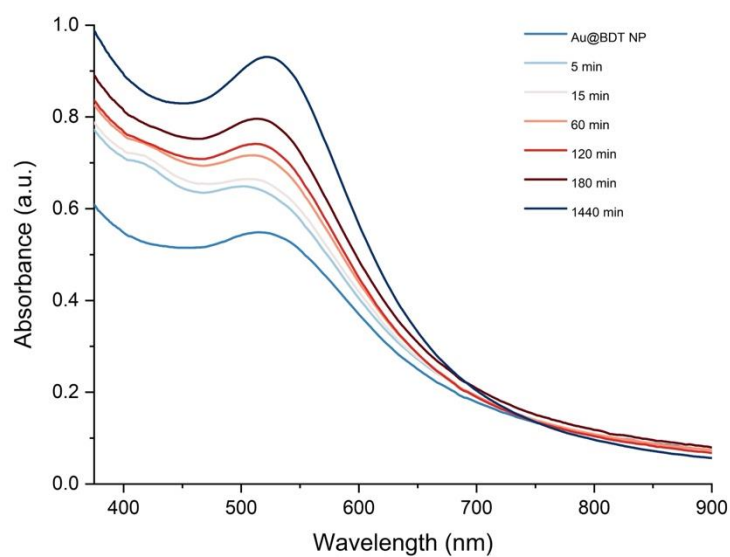


**Figure S26.** Time-dependent optical absorption spectra of the reaction@NP for Au@BDT NP and  $[\text{Ag}_{25}(\text{DMBT})_{18}]^{-}$  NC system.

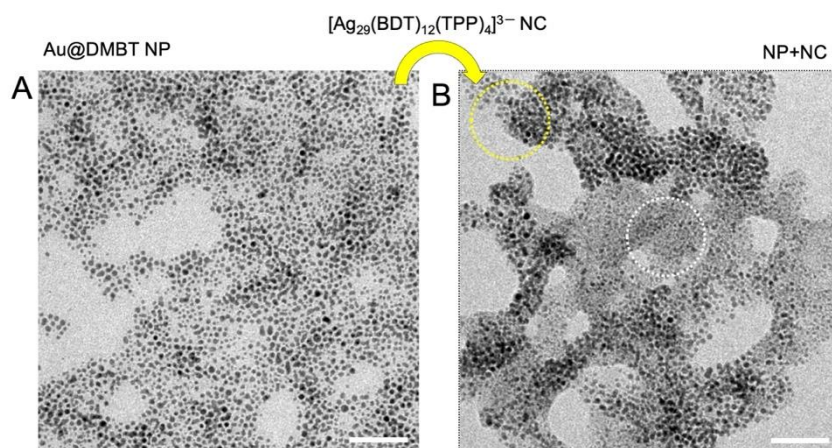


**Figure S27.** Characterization of reaction@NP for Au@DMBT NP and  $[\text{Ag}_{29}(\text{BDT})_{12}(\text{TPP})_4]^{3-}$  NC system. TEM images of the Au@BDT NPs (A) before and (B) after mixing with the NC. The yellow and white encircles correspond to NP- and NC-rich regions, respectively. Scale bar: 50 nm.

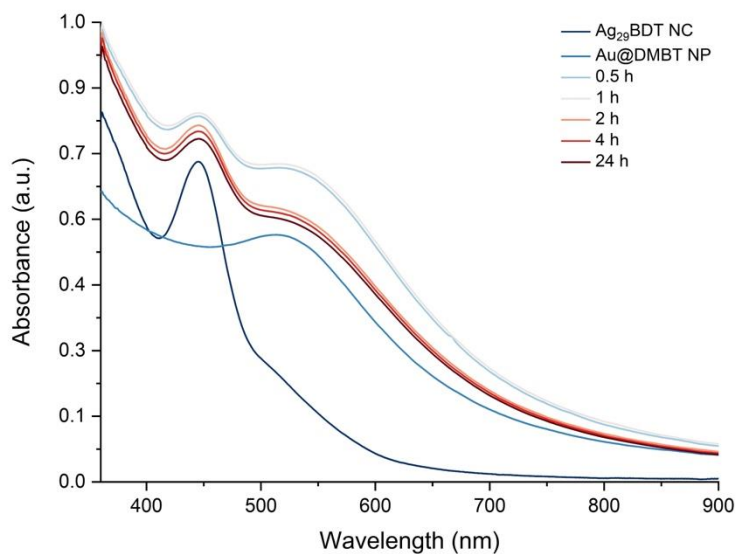


**Figure S28.** Time-dependent optical absorption spectra of the reaction@NP for Au@DMBT NP and  $[\text{Ag}_{29}(\text{BDT})_{12}(\text{TPP})_4]^{3-}$  NC system.

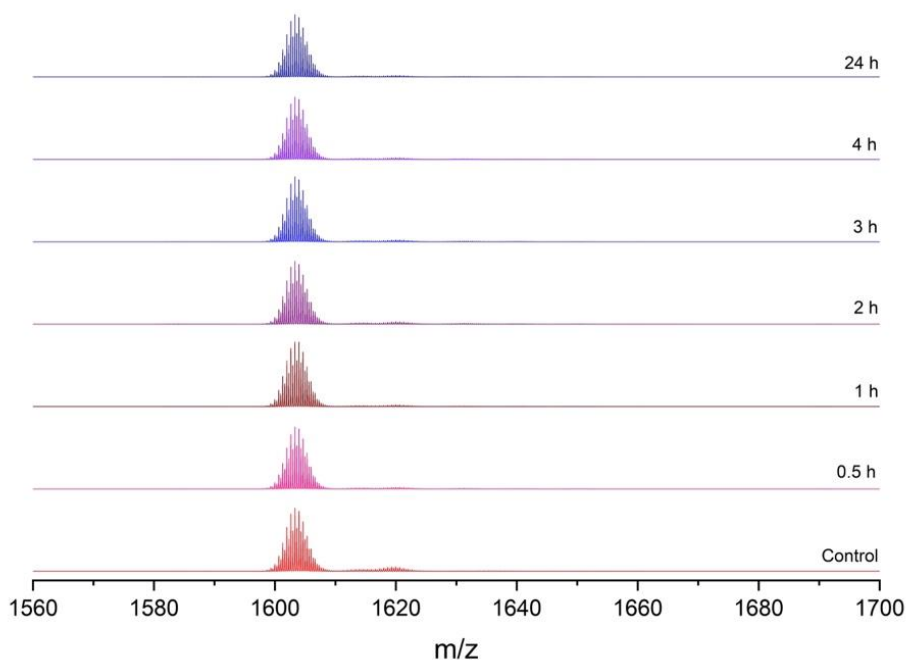


**Figure S29.** ESI mass spectra for the reaction@NC for Au@DMBT NP and  $[\text{Ag}_{29}(\text{BDT})_{12}(\text{TPP})_4]^{3-}$  NC system.

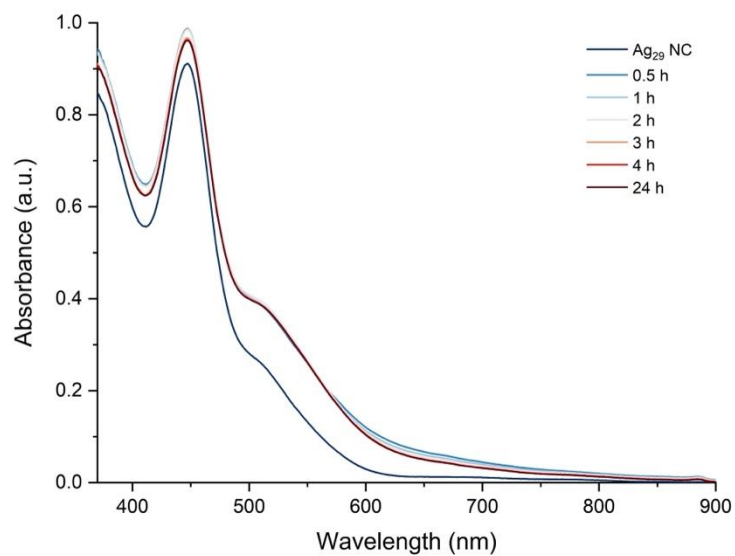


**Figure S30.** Time-dependent optical absorption spectra of the reaction@NC for Au@DMBT NP and  $[\text{Ag}_{29}(\text{BDT})_{12}(\text{TPP})_4]^{3-}$  NC system.

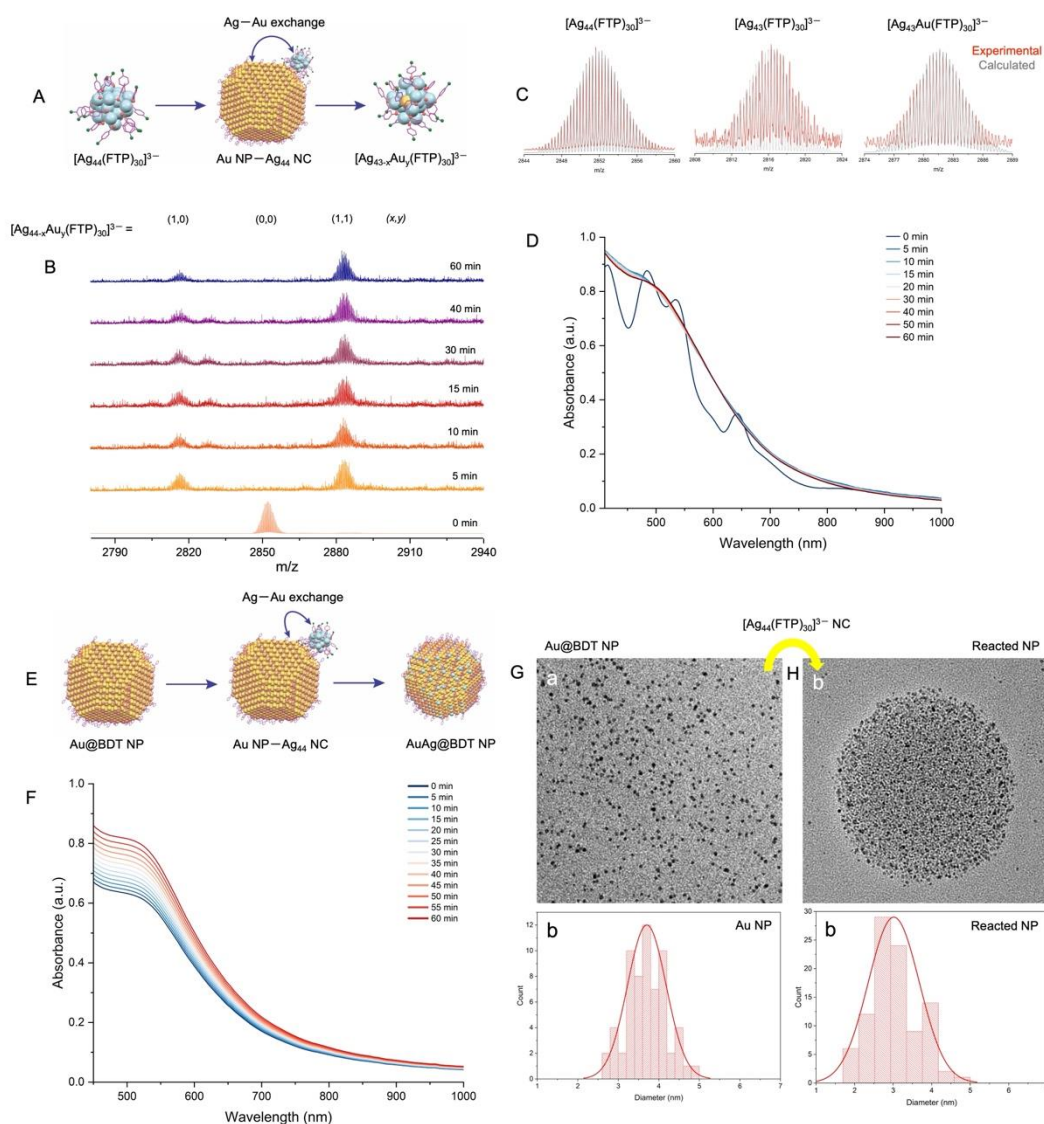


**Figure S31.** Interparticle reaction between Au@BDT NP and  $[Ag_{44}(FTP)_{30}]^{3-}$  NC. For the reaction@NC, (A) the schematic representation of the proposed metal-only exchange pathway as the Ag NC interacts with Au NP, (B) time-dependent ESI MS spectra of the NP-NC reaction, (C) isotopic distribution pattern of the species detected in MS, and (D) the corresponding time-dependent optical absorption spectra of the reaction. For the reaction@NP, (E) the schematic illustration of Au NP – Ag NC reaction mediated Ag-doping of Au@BDT NPs, (F) corresponding time-dependent optical absorption spectra of the reaction, and the TEM images (panel-a) followed by the corresponding particle size distribution (panel-b) of the Au@BDT NPs (G) before and (H) after the reaction. Scale bar: 50 nm. Color code in A and E: Yellow, Au; blue, Ag; pink, S; magenta, C; green, F; H was omitted for clarity.

### SI 3. Computational details

We first generated a (3×4×5) surface unit cell for Au(111) from the bulk Au fcc unit cell with lattice parameter 4.078 Å. We used this small (3×4×5) surface unit cell Au(111) slab for the ligand coverage study with DFT using the CP2K program. Two larger-sized slabs were constructed using this slab by repeating it periodically by specified units in the *x*- and *y*-directions: a medium-sized 2×1 Au(111) slab for DFT reaction energetics and a larger 4×3 slab for DFTB and docking studies. We then placed the DMBT and BDT ligands on the surface of the slabs with varying coverages and orientations. Also, the ligand placement in the models was based on different sites. All these slab constructions were done using ASE (Atomic Simulation Environment) scripts, and ligands were placed using the ASE-GUI program.

We optimized both the Ag NC and 5-layered Au(111)@SR (where SR = 2,4-DMBT and 1,3-BDT) structures individually using the CP2K<sup>6</sup> and the monolayer surfaces only using DFTB+ software packages,<sup>7</sup> respectively. With the optimized Ag NC and Au(111)@SR structures from DFTB+, we carried out the molecular docking of the Ag NC on the Au(111)@SR surface slab models in a grid box of size 126×126×126 points with point spacing 0.375 Å using AutoDock4 software.<sup>8</sup> The docking input files were prepared using AutoDockTools. We used three different levels of theory (software packages in brackets): DFT(CP2K), semi-empirical (DFTB+), and classical force-field (Autodock), with a suitable method (program) being chosen depending on the size of the system due to limited computational resources, and a lack of Slater-Koster parameters for Ag-S interactions in the DFTB+ software package. In DFTB+, the LBFGS (Limited-memory Broyden–Fletcher–Goldfarb–Shanno) optimization scheme was used with the parameters set auorgap-1-1; this set was designed to describe the optical excitations of thiolates on gold NCs.<sup>9–12</sup> D3-dispersion corrections<sup>13</sup> were used with Becke-Johnson damping.<sup>14</sup> The Broyden charge-mixing scheme was used with Fermi smearing to ensure smooth convergence of the SCF calculation.

To compute the Ag/Au atom-exchange energetics between the Ag NC and monolayer Au(111) surfaces, we used the CP2K software package. The Gaussian Plane Wave (GPW) mixed basis-set method was deployed with the plane-wave cutoff of 500 Ry, and DZVP-MOLOPT-GTH (Double-Zeta Valence Polarize (DZVP) molecular optimized (MOLOPT) Goedecker, Teter,

and Hutter (GTH)) basis sets were used with GTH-PBE potentials for all atom types except Au/Ag, while for the Au/Ag atoms, the DZVP-MOLOPT-SR-GTH (SR denotes shorter range) basis set was used. DFT-D3 dispersion corrections were used of Grimme,<sup>13</sup> with Fermi-Dirac smearing and Broyden charge mixing. The PBE (Perdew-Burke-Ernzerhof)<sup>15</sup> exchange-correlation functional was used with an SCF convergence of  $1 \times 10^{-5}$ . The BFGS method with a maximum force of  $4.5 \times 10^{-4}$  Hartree/Bohr was used for geometry optimization.

#### SI 4. Au(111)@SR surface construction

Monomeric DMBT-Au<sub>ad</sub>-DMBT staples and trimeric Au<sub>ad</sub>-BDT-Au<sub>ad</sub>-BDT-Au<sub>ad</sub> chains are the preferred surface arrangements for the 2,4-DMBT and 1,3-BDT monolayers on Au(111), respectively, where Au<sub>ad</sub> denotes a Au(111) surface adatom (Figures S32A and B).<sup>16-19</sup> We arranged the 2,4-DMBT or 1,3-BDT ligands and staples on the Au(111) surface in a hexagonal pattern (Figures S32C) with sulfur atoms anchored at different symmetry sites of the surface while varying the ligand orientations and surface coverages (Figures S33). DFT optimization of Au(111) surface with complete (full) ligand (2,4-DMBT or 1,3-BDT) coverage resulted in distorted structures. Therefore, we assumed the Au(111) surface with a lower ligand coverage for these bulky ligands for our subsequent calculations.

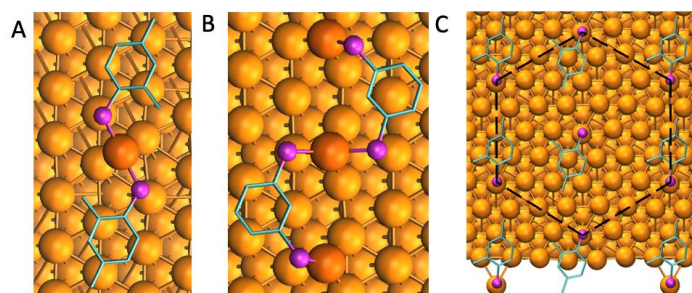


**Figure S32.** Close-up view of (A) a monomeric DMBT-Au<sub>ad</sub>-DMBT staple and (B) a trimeric Au<sub>ad</sub>-BDT-Au<sub>ad</sub>-BDT-Au<sub>ad</sub> chain, on Au(111). (C) The hexagonal pattern of the DMBT monolayer on Au(111). The ball-and-stick spheres for the Au adatom are shown in dark orange, the surface Au atoms in gold, the S atoms in magenta, and the C atoms of the ligands shown in stick representation in cyan.

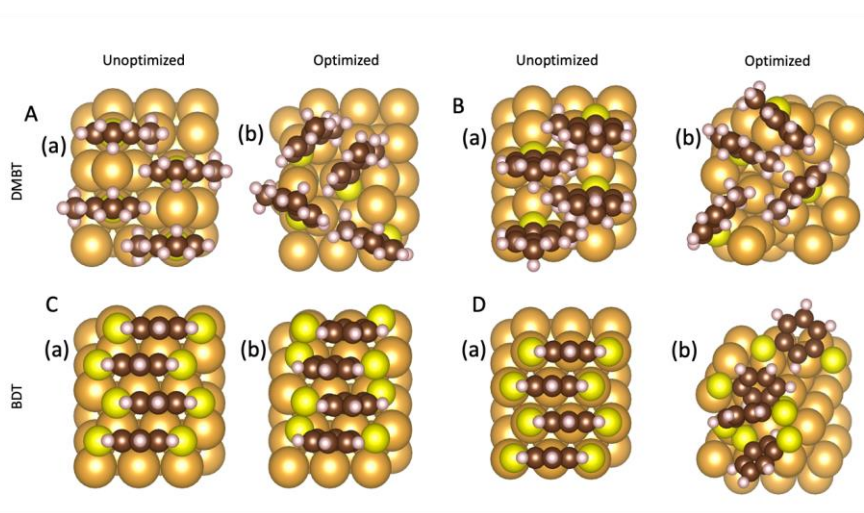


**Figure S33.** Ligand orientations at full coverage on Au(111) ( $3\times 4\times 5$ ) surface unit cell. Unoptimized (a) and their corresponding optimized (b) structures from DFT calculations with (A) a complete coverage of 2,4-DMBT monolayer attached to Au<sub>ad</sub>, with ligands perpendicular and (B) a complete coverage of 2,4-DMBT monolayer attached to Au<sub>ad</sub> with the ligands tilted. (C) a complete coverage of 1,3-BDT monolayer with sulfur atoms attached at hollow sites and (D) a complete coverage of 1,3-BDT monolayer with the sulfur atoms attached at on-top positions. Color code: Gold, Au; yellow, S; brown, C; and white, H.

### SI 5. Ag NC–Au(111)@SR docking interactions

We generated six Au(111) surfaces with different ligand and staple coverages and orientations for docking studies (Figure S34 and details in SI 4). Docking interactions of the  $[\text{Ag}_{25}(\text{DMBT})_{18}]^{-}$  and  $[\text{Ag}_{29}(\text{BDT})_{12}(\text{TPP})_4]^{3-}$  NCs with 2,4-DMBT (Figure 7B) and 1,3-BDT (Figure 7C) monolayered Au(111) surfaces at a low ligand and staple coverage, respectively (interatomic distances are highlighted in the inset). For higher coverage Au(111) surfaces, the docking interactions and orientation of NCs are shown in Figure S35. The docking structures of all six surfaces with the two Ag NCs are provided in Figure S36. Our docking studies revealed that at the lowest ligand coverage, the  $[\text{Ag}_{25}(\text{DMBT})_{18}]^{-}$  NC (Binding Energy, BE =  $-89.39$  kcal/mol) interacts more favorably with the Au(111)@SR surface in comparison to  $[\text{Ag}_{29}(\text{BDT})_{12}(\text{TPP})_4]^{3-}$  NC (BE =  $-79.87$  kcal/mol). The ligand atoms of Ag<sub>25</sub> NC are in close contact with the Au(111) surface ligands and staple atoms at lower coverage, giving in a lower BE for  $[\text{Ag}_{25}(\text{DMBT})_{18}]^{-}$  with Au(111)@DMBT than Ag<sub>29</sub>–Au(111)@BDT system. Additionally, docked structures revealed interligand  $\pi$ - $\pi$  interactions between the stacked

benzene ring of  $\text{Ag}_{25}$  and the surface ligand. With the increase in ligand coverage, however, the NC-surface interaction becomes more favorable as a result of an enhanced  $\pi$ - $\pi$  interaction between the TPP and BDT groups of  $[\text{Ag}_{29}(\text{BDT})_{12}(\text{TPP})_4]^{3-}$  NC and the BDT monolayer of Au(111) surface. About 12 and 6 ligands are involved in the NC-surface  $\pi$ - $\pi$  interaction for the  $\text{Ag}_{25}$ -Au(111)@DMBT and  $\text{Ag}_{29}$ -Au(111)@BDT system, respectively (BE values in Tables S1 and S2).

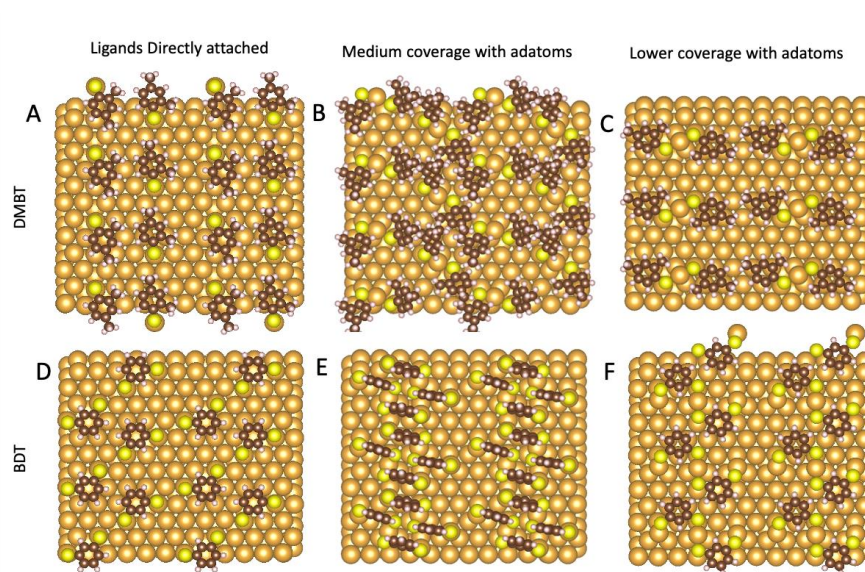


**Figure S34.** DFTB+-optimized Au(111)@SR with a  $4 \times 3$  slab of  $(3 \times 4)$ -surface unit cells with partial ligand coverage. (A)  $[\text{Au}(111)@(\text{DMBT})_{12}]$  surface with sulfur atoms of the 2,4-DMBT ligands attached directly to the on-top position of surface Au atoms (21% coverage) and (B) via adatoms at medium (42%) coverage,  $[\text{Au}(111)@(\text{DMBT}-\text{Au}_{\text{ad}}-\text{DMBT})_{12}]$ , and (C) at lower coverage (21%),  $[\text{Au}(111)@(\text{DMBT}-\text{Au}_{\text{ad}}-\text{DMBT})_6]$ . (D) Au(111) surface with 1,3-BDT ligands attached directly (27% coverage)  $[\text{Au}(111)@(\text{BDT})_{12}]$ , and via ad-atoms with (E) highest coverage (55%),  $[\text{Au}(111)@(\text{Au}_{\text{ad}}-\text{BDT}-\text{Au}_{\text{ad}}-\text{BDT}-\text{Au}_{\text{ad}})_{12}]$ , and (F) lower coverage (27%)  $[\text{Au}(111)@(\text{Au}_{\text{ad}}-\text{BDT}-\text{Au}_{\text{ad}}-\text{BDT}-\text{Au}_{\text{ad}})_6]$ . Color code: Gold, Au; yellow, S; brown, C; and white, H.

## SI 6. Ligand coverage calculations

From concentration calculations in SI 2,

Surface area covered by 2,4-DMBT =  $0.17 \text{ nm}^2$

Surface area covered by 1,3-BDT =  $0.22 \text{ nm}^2$

Surface area of Au(111) 4×3 slab = 9.63 nm<sup>2</sup>

Surfaces A to F, as in Figure S34,

1. Surface A - [Au(111)@(DMBT)<sub>12</sub>]

$$\text{Ligand coverage} = \frac{0.17 \times 12}{9.63} \times 100 \simeq 21\%$$

2. Surface B - [Au(111)@(DMBT-Au<sub>ad</sub>-DMBT)<sub>12</sub>]

$$\text{Ligand coverage} = \frac{0.17 \times 24}{9.63} \times 100 \simeq 42\%$$

3. Surface C - [Au(111)@(DMBT-Au<sub>ad</sub>-DMBT)<sub>6</sub>]

$$\text{Ligand coverage} = \frac{0.17 \times 12}{9.63} \times 100 \simeq 21\%$$

4. Surface D - [Au(111)@(BDT)<sub>12</sub>]

$$\text{Ligand coverage} = \frac{0.22 \times 12}{9.63} \times 100 \simeq 27\%$$

5. Surface E - [Au(111)@(Au<sub>ad</sub>-BDT-Au<sub>ad</sub>-BDT-Au<sub>ad</sub>)<sub>12</sub>]

$$\text{Ligand coverage} = \frac{0.22 \times 24}{9.63} \times 100 \simeq 55\%$$

6. Surface F - [Au(111)@(Au<sub>ad</sub>-BDT-Au<sub>ad</sub>-BDT-Au<sub>ad</sub>)<sub>6</sub>]

$$\text{Ligand coverage} = \frac{0.22 \times 12}{9.63} \times 100 \simeq 27\%$$

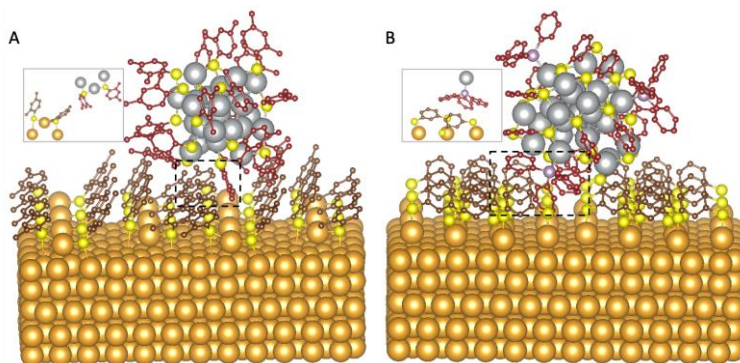


**Figure S35.** Docked NCs on Au(111)@SR with higher coverage monolayers. (A) [Ag<sub>25</sub>(DMBT)<sub>18</sub>]<sup>-</sup> NC on DMBT-monolayered Au(111) surface, and (B) [Ag<sub>29</sub>(BDT)<sub>12</sub>(TPP)<sub>4</sub>]<sup>3-</sup> NC on BDT-monolayered Au(111) surface. Insets show a close-up of

one of the interactions between NC and surface ligands. Color code: Gold, Au; yellow, S; brown, C of surface ligands; gray, Ag; red, C of NC ligands; purple, P of TPP.

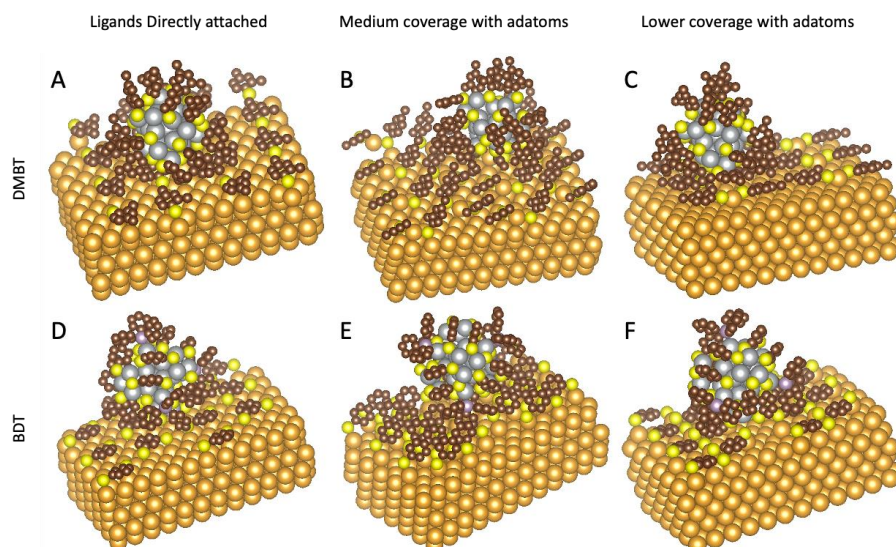


**Figure S36.** Ag NC docking on optimized Au(111)@SR surfaces, where SR refers to 2,4-DMBT or 1,3-BDT ligands. (A) [Au(111)@(DMBT)<sub>12</sub>]@Ag<sub>25</sub>, (B) [Au(111)@(DMBT-Au<sub>ad</sub>-DMBT)<sub>12</sub>]@Ag<sub>25</sub>, and (C) [Au(111)@(DMBT-Au<sub>ad</sub>-DMBT)<sub>6</sub>]@Ag<sub>25</sub>. Au(111) surface with 1,3-BDT directly attached, (D) [Au(111)@(BDT)<sub>12</sub>]@Ag<sub>29</sub>, (E) [Au(111)@(Au<sub>ad</sub>-BDT-Au<sub>ad</sub>-BDT-Au<sub>ad</sub>)<sub>12</sub>]@Ag<sub>29</sub>, and (F) [Au(111)@(Au<sub>ad</sub>-BDT-Au<sub>ad</sub>-BDT-Au<sub>ad</sub>)<sub>6</sub>]@Ag<sub>29</sub>. Color code: Gold, Au; yellow, S; brown, C; gray, Ag; purple, P.

**Table S1.** BE of docked Ag<sub>n</sub>(SR)<sub>m</sub> NCs on Au(111) surface with medium thiolate coverage (refer to Figures S34 and S36).

Complex	BE (kCal/mol)
[Au(111)@(DMBT) <sub>12</sub> ]@Ag <sub>25</sub>	-38.75
[Au(111)@(BDT) <sub>12</sub> ]@Ag <sub>29</sub>	-52.62
[Au(111)@(DMBT-Au <sub>ad</sub> -DMBT) <sub>12</sub> ]@Ag <sub>25</sub>	-11.83
[Au(111)@(Au <sub>ad</sub> -BDT-Au <sub>ad</sub> -BDT-Au <sub>ad</sub> ) <sub>12</sub> ]@Ag <sub>29</sub>	-15.59
Au(111)@Ag <sub>25</sub>	-83.13
Au(111)@Ag <sub>29</sub>	-68.97

Note that, the bare Au(111) surface is represented here as only Au(111).

**Table S2.** BE of docked NCs on Au(111)@SR with different numbers of monolayer staples (refer to Figure S34 and S36, C and F)

No. of Staples	BE (kcal/mol)	BE (kcal/mol)
	[Au(111)@(DMBT-Au <sub>ad</sub> -DMBT)] @Ag <sub>25</sub>	[Au(111)@(Au <sub>ad</sub> -BDT-Au <sub>ad</sub> -BDT-Au <sub>ad</sub> )] @Ag <sub>29</sub>
1	-89.39	-79.87
2	-89.48	-78.23
4	-87.19	-80.81
6	-37.64	-45.20

**Table S3.** DFT calculated energies of parent NCs and Au and Ag atoms

Structure	E <sub>0</sub> (Ha)
Au	-33.1388
Ag	-36.9305
[Ag <sub>25</sub> (DMBT) <sub>18</sub> ] <sup>1-</sup>	-2025.7609
[Ag <sub>29</sub> (BDT) <sub>12</sub> (TPP) <sub>4</sub> ] <sup>3-</sup>	-2229.1081

**Table S4.** Isomers of single gold atom substituted [AuAg<sub>24</sub>(DMBT)<sub>18</sub>]<sup>-</sup> NC

Au location	Isomer	Energy (Ha)
Centre of Icosahedron	C	-2022.0003
Icosahedron	I	-2021.9880
Staple	S	-2021.9858

**Table S5.** Isomers of double gold-atom substituted  $[\text{Au}_2\text{Ag}_{23}(\text{DMBT})_{18}]^- \text{NC}$ 

Au location	Isomer	Energy (Ha)
Icosahedron & Centre of Icosahedron	IC	-2018.2260
Icosahedron & Icosahedron	II	-2018.2143
Icosahedron & Staple	IS	-2018.2129
Staple & Centre of Icosahedron	SC	-2018.2247
Staple & Staple	SS	-2018.2099

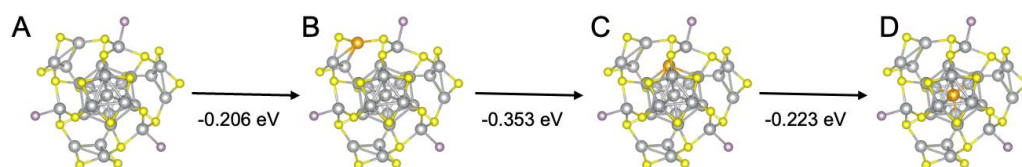


**Figure S37.** Doping pathway of Au atom in  $[\text{Ag}_{29}(\text{BDT})_{12}(\text{TPP})_4]^{3-} \text{NC}$  (A) and reaction energies of intermediate states. The reaction energy is calculated as  $\Delta E = E_{\text{Products}} - E_{\text{Reactants}}$ . The most favorable Au-doping pathway is from the  $\text{Ag}_3\text{S}_3$  motif (B) to the  $\text{Au}_{13}$  icosahedron (C) and finally to the central atom of the core icosahedron position (D). Color code: Gold, Au; yellow, S; gray, Ag; H and C atoms were omitted for clarity.

**Table S6.** Energies of isomers of single gold atom substituted  $[\text{AuAg}_{28}(\text{BDT})_{12}(\text{TPP})_4]^{3-} \text{NC}$ 

Au location	Isomer	Energy (Ha)
Centre of Icosahedron	C	-2225.3452
Icosahedron	I	-2225.3370
Triangular $\text{Ag}_3\text{S}_3$ motif	T	-2225.3240
Bonded to Phosphorus of TPP	P	-2225.3192

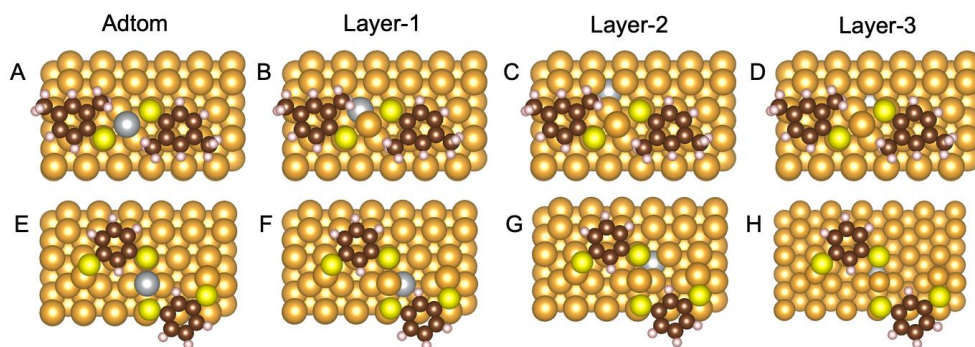


**Figure S38.** Optimized Ag-doped Au(111)  $2 \times 1$  slab of the  $(3 \times 4)$  surface unit cell of 5-layers with a staple of DMBT/BDT, with Ag-atom at various locations for (A-D) [Au(111)@(DMBT-Au<sub>ad</sub>-DMBT)] and (E-H) [Au(111)@(Au<sub>ad</sub>-BDT-Au<sub>ad</sub>-BDT-Au<sub>ad</sub>)]. Different dopant locations on the Au(111) correspond to staple (A, E), layer-1 (B, F), layer-2 (C, G), and layer-3 (D, H). Color code: Gold, Au; yellow, S; gray, Ag; brown, C; and white, H.

#### SI 7. Energies of DFT-optimized Au(111)@SR surfaces

**Table S7.** Energies of undoped Au(111) monolayer surfaces

Structure	$E_0$ (Ha)
[Au(111)@(DMBT-Au <sub>ad</sub> -DMBT)]	-4147.1900
[Au(111)@(Au <sub>ad</sub> -BDT-Au <sub>ad</sub> -BDT-Au <sub>ad</sub> )]	-4205.3797

**Table S8.** Energies of Ag-alloy isomers of [Au(111)Ag@(DMBT-Au<sub>ad</sub>-DMBT)] surface with a single Ag atom (Figure S38A-D)

Ag location	$E$ (Ha)
Staple	-4150.9632
Layer-1	-4150.9696
Layer-2	-4150.9731
Layer-3	-4150.9720

**Table S9.** Ag-alloy isomers of the [Au(111)Ag@(Au<sub>ad</sub>-BDT-Au<sub>ad</sub>-BDT-Au<sub>ad</sub>)] surface with a single Ag-atom (Figure S38E-H)

Ag location	E (Ha)
Staple	-4209.1510
Layer-1	-4209.1604
Layer-2	-4209.1622
Layer-3	-4209.1617

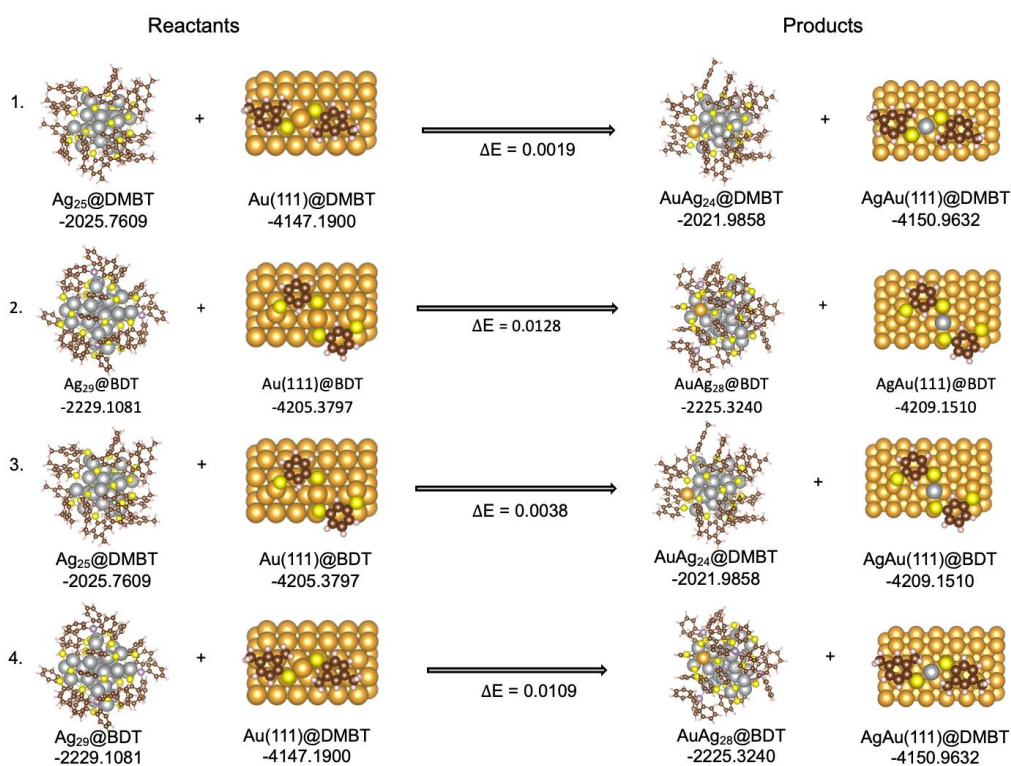


**Figure S39.** Au-Ag atom-exchange reactions between Ag NC – Au(111) monolayer surface and their reaction energies. The reaction energy is calculated as  $\Delta E = E_{\text{Products}} - E_{\text{Reactants}}$ . Note that the above surface energies correspond to Au(111) surface, with 2,4-DMBT or 1,3-BDT ligands attached via Au adatoms. All energies are in Hartree (Ha). Color code: Gold, Au; yellow, S; gray, Ag; brown, C; and white, H.

## SI 8. References

- (1) Brust, M.; Walker, M.; Bethell, D.; Schiffrin, D. J.; Whyman, R. Synthesis of Thiol-Derivatised Gold Nanoparticles in a Two-Phase Liquid–Liquid System. *J. Chem. Soc. Chem. Commun.* **1994**, No. 7, 801–802.
- (2) Joshi, C. P.; Bootharaju, M. S.; Alhilaly, M. J.; Bakr, O. M. [Ag<sub>25</sub>(SR)<sub>18</sub>]<sup>-</sup>: The “Golden” Silver Nanoparticle. *J. Am. Chem. Soc.* **2015**, *137* (36), 11578–11581.
- (3) AbdulHalim, L. G.; Bootharaju, M. S.; Tang, Q.; Del Gobbo, S.; AbdulHalim, R. G.; Eddaoudi, M.; Jiang, D. E.; Bakr, O. M. Ag<sub>29</sub>(BDT)<sub>12</sub>(TPP)<sub>4</sub>: A Tetravalent Nanocluster. *J. Am. Chem. Soc.* **2015**, *137* (37), 11970–11975.
- (4) Krishnadas, K. R.; Ghosh, A.; Baksi, A.; Chakraborty, I.; Natarajan, G.; Pradeep, T. Intercluster Reactions between Au<sub>25</sub>(SR)<sub>18</sub> and Ag<sub>44</sub>(SR)<sub>30</sub>. *J. Am. Chem. Soc.* **2016**, *138* (1), 140–148.
- (5) Bose, P.; Chakraborty, P.; Mohanty, J. S.; Nonappa; Ray Chowdhuri, A.; Khatun, E.; Ahuja, T.; Mahendranath, A.; Pradeep, T. Atom Transfer between Precision Nanoclusters and Polydispersed Nanoparticles: A Facile Route for Monodisperse Alloy Nanoparticles and Their Superstructures. *Nanoscale* **2020**, *12* (43), 22116–22128.
- (6) Kühne, T. D.; Iannuzzi, M.; Del Ben, M.; Rybkin, V. V.; Seewald, P.; Stein, F.; Laino, T.; Khaliullin, R. Z.; Schütt, O.; Schiffmann, F. CP2K: An Electronic Structure and Molecular Dynamics Software Package-Quickstep: Efficient and Accurate Electronic Structure Calculations. *J. Chem. Phys.* **2020**, *152* (19), 194103.
- (7) Hourahine, B.; Aradi, B.; Blum, V.; Bonafé, F.; Buccheri, A.; Camacho, C.; Cevallos, C.; Deshayé, M. Y.; Dumitrică, T.; Dominguez, A.; Ehlert, S.; Elstner, M.; van der Heide, T.; Hermann, J.; Irlé, S.; Kranz, J. J.; Köhler, C.; Kowalczyk, T.; Kubař, T.; Lee, I. S.; Lutsker, V.; Maurer, R. J.; Min, S. K.; Mitchell, I.; Negre, C.; Niehaus, T. A.; Niklasson, A. M. N.; Page, A. J.; Pecchia, A.; Penazzi, G.; Persson, M. P.; Řezáč, J.; Sánchez, C. G.; Sternberg, M.; Stöhr, M.; Stuckenberg, F.; Tkatchenko, A.; Yu, V. W. - z.; Frauenheim, T. DFTB+, a Software Package for Efficient Approximate Density Functional Theory Based Atomistic Simulations. *J. Chem. Phys.* **2020**, *152* (12), 124101.
- (8) Morris, G. M.; Goodsell, D. S.; Halliday, R. S.; Huey, R.; Hart, W. E.; Belew, R. K.; Olson, A. J. Automated Docking Using a Lamarckian Genetic Algorithm and an Empirical Binding Free Energy Function. *J. Comput. Chem.* **1998**, *19* (14), 1639–1662.

- (9) Elstner, M.; Porezag, D.; Jungnickel, G.; Elsner, J.; Haugk, M.; Frauenheim, Th.; Suhai, S.; Seifert, G. Self-Consistent-Charge Density-Functional Tight-Binding Method for Simulations of Complex Materials Properties. *Phys. Rev. B* **1998**, *58* (11), 7260–7268.
- (10) Niehaus, T. A.; Elstner, M.; Frauenheim, Th.; Suhai, S. Application of an Approximate Density-Functional Method to Sulfur Containing Compounds. *J. Mol. Struct. THEOCHEM* **2001**, *541* (1), 185–194.
- (11) Fihey, A.; Hettich, C.; Touzeau, J.; Maurel, F.; Perrier, A.; Köhler, C.; Aradi, B.; Frauenheim, T. SCC-DFTB Parameters for Simulating Hybrid Gold-Thiolates Compounds. *J. Comput. Chem.* **2015**, *36* (27), 2075–2087.
- (12) Vuong, V. Q.; Madrdejós, J. M. L.; Aradi, B.; Sumpter, B. G.; Metha, G. F.; Irle, S. Density-Functional Tight-Binding for Phosphine-Stabilized Nanoscale Gold Clusters. *Chem. Sci.* **2020**, *11* (48), 13113–13128.
- (13) Grimme, S.; Antony, J.; Ehrlich, S.; Krieg, H. A Consistent and Accurate Ab Initio Parametrization of Density Functional Dispersion Correction (DFT-D) for the 94 Elements H-Pu. *J. Chem. Phys.* **2010**, *132* (15), 154104.
- (14) Grimme, S.; Ehrlich, S.; Goerigk, L. Effect of the Damping Function in Dispersion Corrected Density Functional Theory. *J. Comput. Chem.* **2011**, *32* (7), 1456–1465.
- (15) Hammer, B.; Hansen, L. B.; Nørskov, J. K. Improved Adsorption Energetics within Density-Functional Theory Using Revised Perdew-Burke-Ernzerhof Functionals. *Phys. Rev. B* **1999**, *59* (11), 7413–7421.
- (16) Maksymovych, P.; Sorescu, D. C.; Yates, J. T. Gold-Adatom-Mediated Bonding in Self-Assembled Short-Chain Alkanethiolate Species on the Au(111) Surface. *Phys. Rev. Lett.* **2006**, *97* (14), 146103.
- (17) Cossaro, A.; Mazzarello, R.; Rousseau, R.; Casalis, L.; Verdini, A.; Kohlmeier, A.; Floreano, L.; Scandolo, S.; Morgante, A.; Klein, M. L.; Scoles, G. X-Ray Diffraction and Computation Yield the Structure of Alkanethiols on Gold(111). *Science* **2008**, *321* (5891), 943–946.
- (18) Häkkinen, H. The Gold–Sulfur Interface at the Nanoscale. *Nat. Chem.* **2012**, *4* (6), 443–455.
- (19) Kestell, J.; Abuflaha, R.; Garvey, M.; Tysoe, W. T. Self-Assembled Oligomeric Structures from 1,4-Benzenedithiol on Au(111) and the Formation of Conductive Linkers between Gold Nanoparticles. *J. Phys. Chem. C* **2015**, *119* (40), 23042–23051.